Integrated design of third generation concentrated solar power plants under uncertainty

by

Karthik Rajasekaran

B.S. Chemical Engineering, Tulane University, 2007

Submitted to the System Design and Management Program
in partial fulfillment of the requirements for the degree of

Master of Science in Engineering and Management

at the

MASSACHUSETTS INSTITUTE OF TECHNOLOGY

May 2022

Author .....
System Design and Management Program
May 19, 2022

Certified by .....
Olivier L. de Weck
Professor of Aeronautics and Astronautics and Engineering Systems
Thesis Supervisor

Certified by .....
Richard de Neufville
Professor of Engineering Systems
Thesis Supervisor

Accepted by .....
Joan S. Rubin
Executive Director, System Design and Management Program

Integrated design of third generation concentrated solar power plants under uncertainty

by

Karthik Rajasekaran

Submitted to the System Design and Management Program
on May 19, 2022, in partial fulfillment of the
requirements for the degree of
Master of Science in Engineering and Management

Abstract

This research focuses on the Gen3 (3rd generation) solar tower CSP (concentrated solar power) variant. A methodology is introduced to evaluate two different approaches to deploying this technology - one is the conventional "build large" approach and the other is a "build modular" approach. Performance and cost models of the two different approaches are built and validated against industry data and then the two different approaches compete across three locations (Daggett CA, New Orleans LA, and Boston MA) and three different capacity factors (20%, 30%, and 40%). For these nine cases, the comparison between the two different approaches is first done with deterministic inputs and then with stochastic inputs for selected variables.

The results show that when the "build large" approach is compared against the "build modular" approach using deterministic inputs, the "build large" approach" is favored and has a NPV that is 5%-15% higher than that of the "build modular" approach for most of the nine cases, which aligns with the current industry belief that the "build large" approach is better due to economies of scale. However, when the same approaches are compared using stochastic inputs, the "build modular" approach is preferred over the "build large" approach. The ENPVs for the "build modular" approach are 20% higher than that of the "build large" approach while requiring 50% less initial capital than the "build large" approach. This reversal is driven primarily by the flexibility and the learning rate inherent to the "build modular" approach. By employing a "build modular" approach for this technology, a firm that is entering the CSP market could gain a competitive advantage over other firms in the CSP and renewable energy markets.

Thesis Supervisor: Olivier L. de Weck
Title: Professor of Aeronautics and Astronautics and Engineering Systems

Thesis Supervisor: Richard de Neufville
Title: Professor of Engineering Systems

Acknowledgments

This document marks the conclusion of a journey that I started 13 years ago. The past few years at MIT have been everything I originally hoped for and more. MIT's System Design and Management program has been a transformative experience for me.

Thank you to my wife, Rubini, and our baby boy, Aadhav. Rubini, thank you for all of the support, it would not have been possible without you, and that is no platitude - the fact we have made it through while both staying employed and welcoming a new member to our family is an accomplishment in itself. Aadhav, if you're reading this in the future, I love you. You were born here, on a cold day in January! Thank you for adapting to our small but cozy apartment in the Westgate high-rise. I will forever remember our time here at MIT as the first place we lived as a family.

Thank you to my mom and dad, Sasiprabha and Kanniah. I love you both always. You have always been there and supported me in every way since I was born. It was a long journey to get here and you were behind me through all of the ups and downs. You have been the biggest factor in my successes, and I will forever be grateful for everything you have done for us. I would not be where I am today without you both.

Thank you to my brother, Senthil. I always appreciated the spirited advice you've given me and the conviction with which you gave it. I look forward to more of that. I will always be here for you.

Thank you to my advisors, Professors Olivier de Weck and Richard de Neufville, for guiding me on my thesis journey - I definitely started at square one and learned a lot along the way. Your classes were my absolute favorite and your love for teaching really showed through.

Finally, thank you to Bryan Moser, SDM's Academic Director, and Joan Rubin, SDM's Executive Director, for welcoming me to the SDM family and for guiding me through the program. I showed up in the summer of 2019 with almost zero background and you helped me find my place and thrive at MIT.

Contents

List of Figures

List of Tables

Acronyms

CF Capacity factor

CSP Concentrating solar power

DCF Discounted cash flow

DNI Direct Normal Irradiance

ENPV Expected net present value

Gen1 1st generation, referring to a solar tower-based CSP design

Gen2 2nd generation, referring to a solar tower-based CSP design

Gen3 3rd generation, referring to a solar tower-based CSP design

GHG Greenhouse gases

LCOE Levelized cost of electricity (typically USD/kWh)

LCOS Levelized cost of storage (typically USD/kWh)

LMTD Log mean temperature difference

LR Learning rate

NASA National Aeronautics and Space Administration

NPV Net present value

NREL National Renewable Energy Laboratory

NSRDB National Solar Radiation Database

PI Proportional - integral

PID Proportional - integral - derivative

PR Progress ratio

PV Photovoltaics

SAM System Advisor Model

sCO$_2$ Supercritical carbon dioxide

TES Thermal energy storage

TIT Turbine inlet temperature

TMY Typical meteorological year

TRL Technology Readiness Level

TTD Terminal temperature difference, or $T_{hotside,out}$-$T_{coldside,in}$ as defined by [21]

Chapter 1

Introduction

1.1 Motivation

Due to the increasing effects of human-made climate change, there has never been a greater need for sources of renewable energy that can both support society's global energy demands and substantially reduce (or even eliminate) GHG emissions. In order for these sources of renewable energy to displace existing conventional hydrocarbon-based sources of energy such as coal and natural gas, renewable energy must not only be economically competitive with conventional sources but also be able to match the ability of conventional sources to generate power around the clock.

Out of the many different renewable energy technologies under development today, the highest profile technologies that have shown the most growth in installed capacity in recent years are wind and solar PV. Between 2012 and 2021, the worldwide electrical generation capacity from wind energy tripled while solar PV octupled [2]. The rapid growth in installed capacity for these two technologies correlates well with significant reductions in the LCOE of wind and solar PV over the same period. Today, relative to conventional sources, wind and solar PV are already competitive and are starting to become outright cheaper on a LCOE basis [1].

However, the LCOE does not account for the ability to provide power around the clock. Unfortunately, wind and solar PV are not yet able to generate power around the clock in a cost-effective manner. For solar PV, when the cost of storage

is included, the LCOS increases to values that are not competitive with conventional sources [25]. The reason for this is that both wind and solar PV convert energy (wind and solar, respectively) directly into electricity. Except for a few unique areas on the Earth, neither does the sun shine nor the wind blow at high speeds for 24 hours per day year-round. Therefore in order to provide power around the clock, the electricity needs to be stored, and the current technologies to do so are very expensive. This causes both wind and solar PV to be noncompetitive with fossil fuels once the cost of electricity storage is included.

There is still a need for a source of renewable energy that can generate power around the clock while remaining competitive with conventional sources. One potential promising technology that has the potential to meet both conditions is CSP. CSP is similar to solar PV in that both utilize solar energy. However, while solar PV converts solar energy directly to electricity using the photovoltaic effect, CSP initially converts solar energy into thermal energy. Then, depending on the application, either the thermal energy is used as-is to generate products like steam or it can be converted into other valued products such as electricity. By converting solar energy into thermal energy first, CSP can make use of inexpensive technologies designed to store heat instead of expensive technologies to store electricity.

Although CSP has the inherent advantage of cheaper energy storage over solar PV, it has not taken off nearly as fast as solar PV. Between 2012 and 2021, the worldwide electrical energy capacity of CSP increased by 2.5x. However, in 2021, the worldwide electrical generation capacity of solar PV was 843 GW vs 6.4 GW for CSP, a difference of 132x [2].

There are two reasons why there is such a large disparity between the installed capacities of solar PV and CSP to date. The first is that there have been tremendous improvements to the cost and performance of solar PV panels in the last 20 years as evidenced in the rapid reduction in LCOE of solar PV over this time period [1]. Note that while battery technology has also improved, it is still too expensive to cost effectively store electrical power for use around the clock at a large scale. Second, CSP has historically been built as large utility-scale installations. As a result, the amount

of engineering and capital investment required for CSP plants has been much higher than that of solar PV plants for similar electricity generation capacity, if the ability to produce around the clock is disregarded. This has discouraged the proliferation of CSP capacity relative to solar PV capacity, which has been installed from the utility scale to the residential household scale. As a result of these two reasons, CSP has largely been neglected except at a limited implementation in a handful of countries while solar PV is nearly ubiquitous across the world.

One factor to note that may contribute to the two reasons mentioned above is the fact that CSP is not architecturally stable yet compared to solar PV. With solar PV, even through the internals and their performance have changed over time, the form is consistent - panels of varying size. However, with CSP, although the principle of converting solar energy to thermal energy is consistent, the forms this technology can take vary significantly. This will be covered in detail in section 2.1.

In the end, the fight against climate change is still in need for a renewable energy source that can be economically competitive with conventional sources while being able to generate power around the clock. Although CSP has been passed up initially in favor of solar PV and wind, it may yet still be able to meet this need first. As to whether CSP is on a track to meet this need or not, the first question is whether CSP can achieve the same rate of improvement that solar PV has in the past years. The second question is whether the historical practice of building CSP in large utility-scale installation still makes sense or if a new approach is needed.

1.2 Thesis Objectives and Approach

The purpose of this research is to contrast the current approach to CSP, which is to build large plants, with a more modular approach. Before system models can be generated, a particular variant of CSP is selected, a Gen3 CSP plant (see section 2.1). Then, to perform this comparison, system models of Gen3 CSP plants will be developed to estimate the performance characteristics of the different approaches. A literature review will be conducted to collect realistic design parameters and rules of

thumb to inform the selection of parameters that govern the behavior of the different components in the system models. Outputs from the system model will be used to estimate the cost of the Gen3 CSP plants, drawing on correlations available in literature. The cost and performance characteristics of the Gen3 CSP plant (from the system model and the cost) will then be used as inputs to calculate NPV using a DCF approach and deterministic inputs. Finally, in recognition of the significant uncertainty in the design, cost, and other system parameters for CSP plants in general, the NPV calculation will be done using stochastic inputs for selected variables to account for the uncertainties. Using the outputs of the stochastic NPV calculation, a multidimensional comparison between the current "build large" approach and a "build modular" approach will be performed for the Gen3 solar tower CSP variant. The calculation of NPV using a DCF approach using deterministic and stochastic inputs follows the methodology proposed by de Neufville and Scholtes [9].

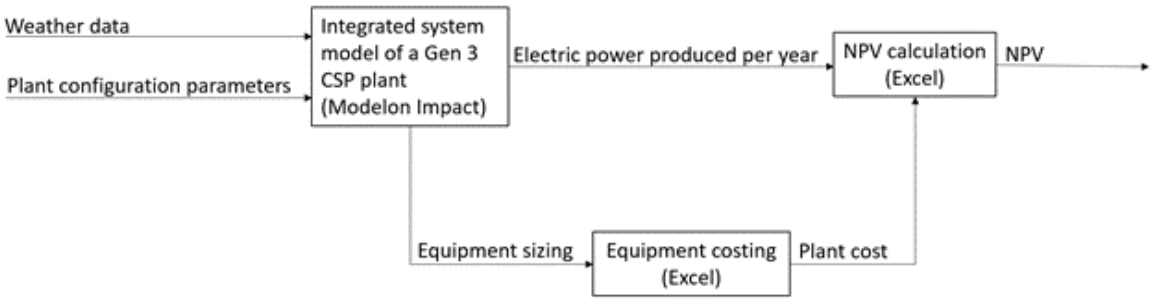

Figure 1-1: High level block diagram of the approach

The equipment costing and NPV calculations will be performed in Excel. The system model will be done in Modelon Impact. Modelon Impact is a commercial implementation of Modelica and it has several advantages over other platforms. First, Modelon Impact comes with a set of libraries that serve a wide range of industries and are continuously validated and vetted by Modelon, the parent company. OpenModelica, a free version of Modelica, also has libraries, but these are developed by users and may not be vetted to the same degree as the Modelon Impact libraries. Compared to other system simulation tools, Modelon Impact has the ability to simulate the transient behavior of both hardware and software (i.e. control logic), which is important for keeping track of the states of the components in the CSP plant over

the course of the simulation. In addition to the components provided in the libraries, Modelon Impact/Modelon come with the ability to design custom components based on equations or correlations. The ability to design custom components is important for modeling CSP plants, where some components are specialized and not very well known outside of the CSP industry. Lastly, Modelon Impact has a graphical user interface, which is very helpful for visualizing, building, and modifying a system model with multiple interlinked components.

1.3 Key Research Questions

- Under what conditions is a "build modular" approach to CSP better than a "build large" approach for a Gen3 solar tower CSP plant?
- Is the "build modular" approach better than the "build large" approach in three different locations in the US?
- What are the most important uncertainties in a technoeconomic evaluation (using NPV) of a Gen3 solar tower CSP plant?
- What is the expected performance and cost of a Gen3 solar tower CSP plant given a location and design parameters available in literature?

1.4 Thesis Structure

- Chapter 1 - Introduction: This chapter summarizes the motivation for the research in this work, and the importance of this research to the CSP industry. It defines the research objectives, the approach, and key questions to be address by the research.
- Chapter 2 - Literature review: This chapter summarizes the current state of CSP and more specifically Gen3 solar tower CSP in literature. It also identifies approaches and assumptions in literature to modeling the performance of Gen3 solar tower CSP plants and where there are potential gaps.

- Chapter 3 - Methodology: This chapter defines the "build large" and "build modular" approaches and the different cases over which they are compared. It describes the process of building and validating performance models and cost models of Gen3 solar tower CSP plants. It also describes the process of a NPV analysis with both deterministic and stochastic inputs.

- Chapter 4 - Results: This chapter describes the outputs of the Gen3 solar tower CSP plant performance models and cost models. The results of the comparison between the "build large" and "build modular" approaches for different cases are presented in visuals and discussed.

- Chapter 5 - Conclusion: This chapter summarizes the insights and takeaways from Chapter 4 - Results from the perspective of a firm that wants to enter the CSP market and is deciding between choosing a "build large" or a "build modular" approach. Areas of opportunity for future work are also introduced.

Chapter 2

Literature Review

2.1 The current state of CSP

CSP has been around for hundreds, if not thousands of years [8], but it is still a relatively immature technology compared to solar PV. Although this is a subjective assessment, one marker to support this assessment is compare total installed electricity generation capacity to date between the two sources:

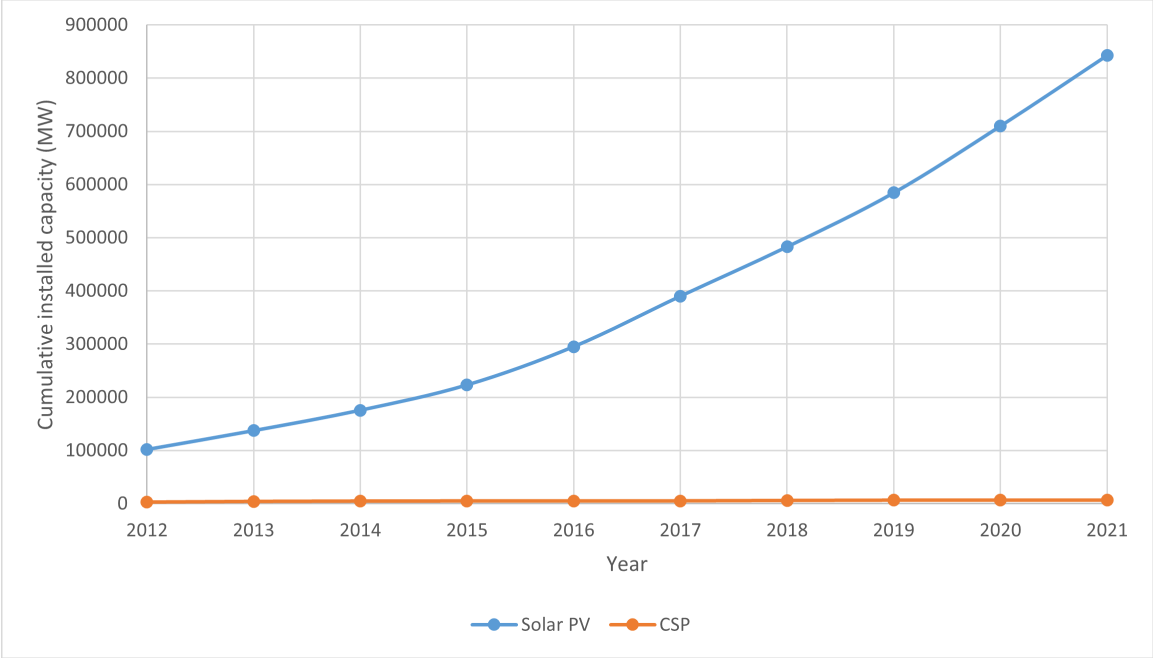

Figure 2-1: The cumulative installed capacity of solar PV is orders of magnitude higher than that of CSP to date. Data from IRENA [2]

.

The installed capacity of solar PV has been increasing exponentially over the past decade, while the installed capacity of CSP has not. If both technologies were put on a conceptual S-curve as per below,

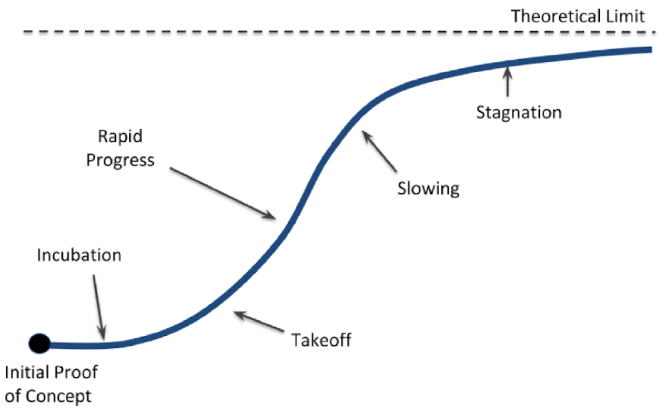

Figure 2-2: Conceptual stages along the S-Curve of a technology [10]

.

then it makes the most sense to classify solar PV as either in the "Takeoff" or "Rapid Progress" stages, while CSP is likely close to the incubation section of the curve. For a technology like CSP that is still close to the incubation section of the curve, it is reasonable to expect that the technology is not very stable architecturally. This is indeed the case for CSP. As a reference point, compare how solar PV panels have changed from 1884 to 2022 in figure 2-3.

(a) Solar panels in New York City in 1884 [27]

(b) Solar array on a house in 2022 [27]

Figure 2-3: The form of solar PV hasn't changed much in over 100 years.

However, with CSP, there are at least four different variants, as shown in figure 2-4.

The difference between the four variants is best characterized by how the heat transfer

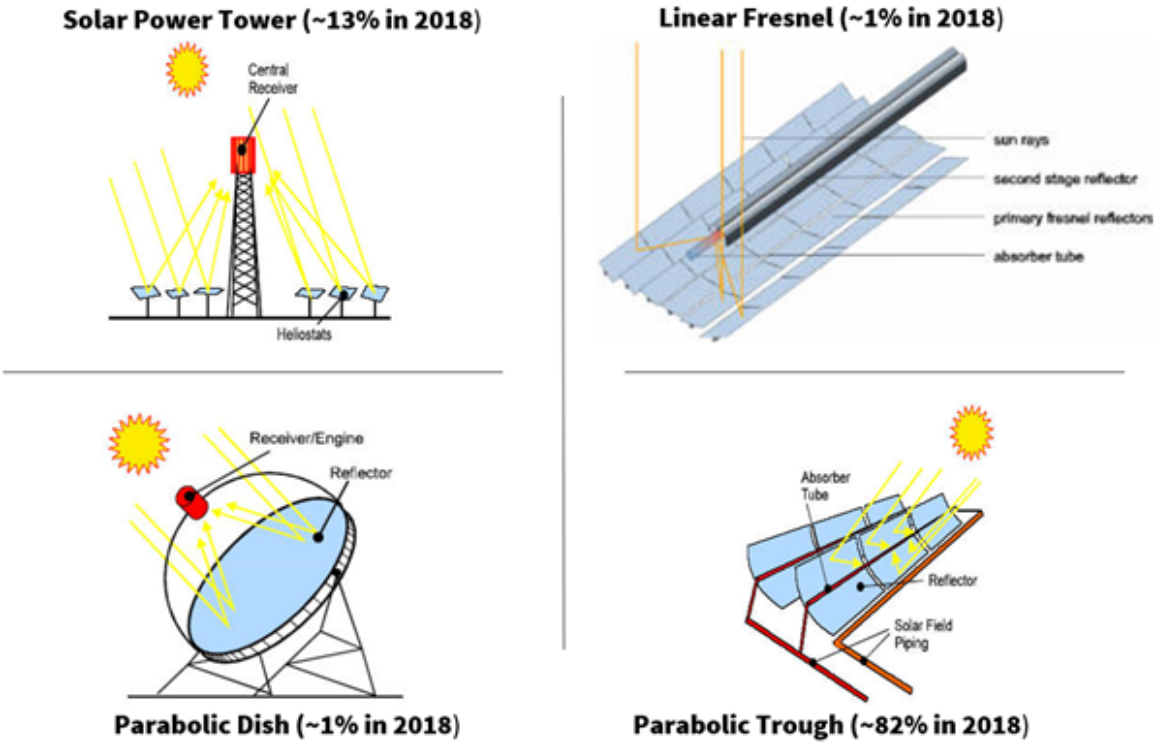

Figure 2-4: Four of the most well known variants of CSP, with their approximate installed ratios in 2018 from [22] and images from [35].

medium moves and where the electrical power is generated (while CSP can be used to generate other forms of power, the majority of CSP installations to date have been used to generate electricity).

- Parabolic dish - the heat transfer medium is contained within a receiver for each reflector. Power is generated immediately adjacent to the receiver using a miniature Stirling or Brayton cycle engine. As a result, the generation of power for a field of reflectors is distributed across all of the reflectors. This type of CSP system is capable of attaining high temperatures immediately at the receiver because the heat transfer medium does not need to travel very far. However, since everything is located within the space of each reflector, there is no way to store thermal energy.

- Parabolic trough - the heat transfer medium, typically a thermal oil, is pumped from a central location to each trough and back to the central location. Power is

generated at the central location, typically by transferring the heat from the oil to a conventional steam cycle to generate electricity. The heat transfer medium travels to and from the central location to all of the troughs. Thermal energy storage is possible at the central location. This is the most common type of CSP plant.

- Solar power tower (or solar tower for short) - the heat transfer medium is contained in a central tower and only travels vertically within the tower. Power is generated centrally within the tower. At the top of the tower, the heat transfer medium is heated, and falls towards the bottom of the tower where it transfers its heat to a power cycle. The cold heat transfer medium is elevated back up to the top of the tower to repeat the cycle. Thermal energy storage is possible in the tower. This is the second most common type of CSP plant.

- Linear fresnel - similar to the long arrays of the parabolic trough, however these mirrors are flat rather than curved. Just like the parabolic trough concept, the heat transfer medium is pumped from a central location through a pipe that above the mirrors. The heat transfer medium is heated as it passes through the pipe before returning to a central location where its heat is transferred to a cycle (typically steam) to generate electricity. Just like the parabolic trough concept, thermal energy storage is possible at the central location.

The solar tower concept is of particular interest for this work because the power is generated at a central location and doesn't require the movement of the heat transfer medium across long horizontal distances to each of the reflectors/mirrors (especially if the plant is designed to produce power at the megawatt level and above). As a result, the solar tower concept can operate at high temperatures without worrying about thermal losses incurred from the horizontal transport of the heat transfer medium and the high costs of materials required to minimize these thermal losses. Furthermore, with a centralized power generation point, the solar tower can take advantage of economies of scale in cost and efficiency in the power generation subsystem, since the costs of the equipment in the power generation subsystem scale sublinearly with the

performance of the equipment. Last but not least, it is capable of thermal energy storage in the tower.

Despite these advantages, the majority of installed CSP capacity over the past decade has been parabolic trough as seen in figure 2-5. The solar tower concept has only recently become relatively more popular. Note also the majority of projects shown in the figure have thermal energy storage for only up to 8 hours.

Figure 5.2 CSP total installed costs by project size, collector type and amount of storage, 2010-2020

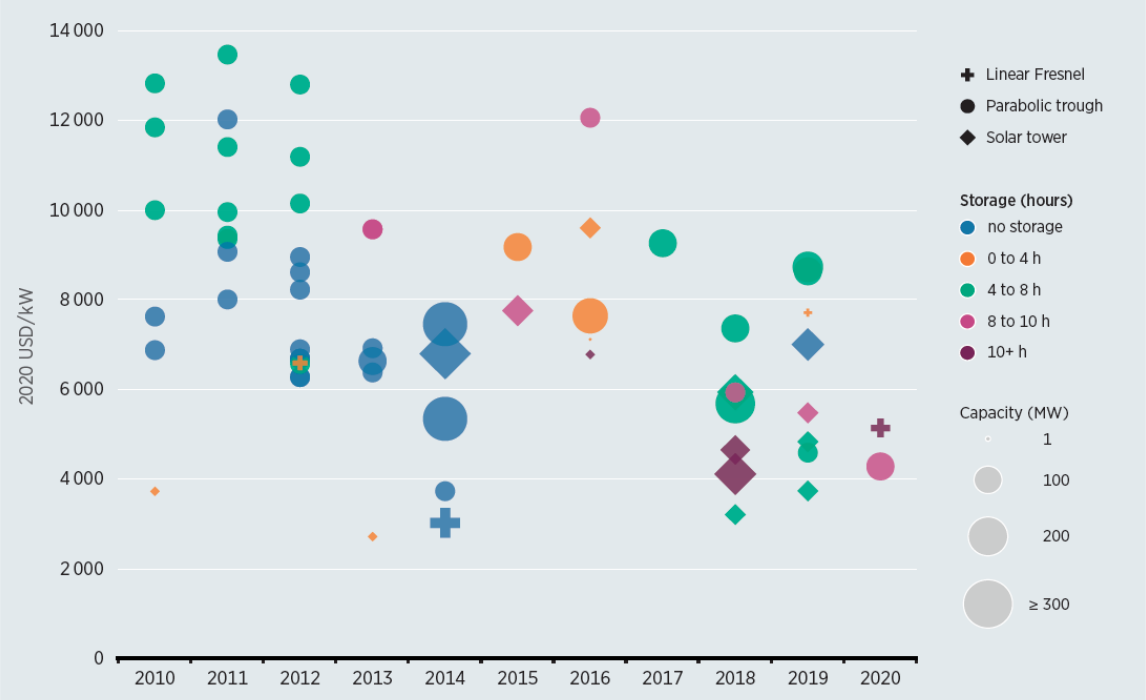

Source: IRENA Renewable Cost Database.

Note: Only projects in the database with information available for all the variables displayed are shown. Data can therefore diverge from the global dataset.

Figure 2-5: Solar towers (the diamonds) have only become more common fairly recently, and even then only a few have thermal energy storage above 8 hours. [1]

.

2.2 About solar tower CSP

Even within the solar tower concept, there are multiple variants. These variants are distinguished by the choice of heat transfer medium.

- Solar tower CSP Gen1 - The first generation uses water as the heat transfer

medium. The maximum temperature achievable for the Gen1 cycle is around 550 °C, referencing the maximum temperature at the Ivanpah Solar Power Facility [47]. On the plus side, the steam cycle used in this variant is familiar to most utility operators, but the cost of the plant is expensive due to the materials required to contain water at these temperatures.

- Solar tower CSP Gen2 - The second generation uses molten salts as the heat transfer medium. The maximum temperature available for the Gen2 cycle is around 565°C, referencing the maximum temperature at the Crescent Dunes Solar Energy Plant [28]. The maximum temperature is slightly improved over the Gen1 cycle and the molten salts offer some better heat transfer properties than water, but there are still expenses in managing the corrosivity of the molten salts and the systems required to keep the salts molten.

- Solar tower CSP Gen3 - The third generation uses particles, which are similar to sand, as the heat transfer medium. The Gen3 cycle is capable of a maximum temperature of 800+°C [37]. These particles are relatively easy to store and manage compared to the Gen2 variant and also do not require high pressures like the Gen1 variant. However, this variant has not been implemented commercially yet.

One dimension by which these variants can be compared is by their maximum temperature. Since the heat transfer fluid is used to provide heat to the power generation subsystem, it follows that the higher the maximum temperature of the heat medium, the higher the maximum temperature of power generation subsystem. The approximate effect of increasing the maximum temperature of the power generation subsystem on the efficiency of the cycle can be determined using an estimated efficiency derived from the formula for the efficiency of a Carnot cycle:

$$\eta = 1 - \sqrt{\frac{T_{min}}{T_{max}}}$$

Where η is the cycle efficiency, T_{min} is the minimum temperature (in Kelvin) in the

cycle where the heat is rejected, and T_{max} is the maximum temperature (in Kelvin) in the system. As a simplification, T_{min} is assumed to be the standard sea level temperature (20°C = 293.15 K).

A second dimension by which to compare these variants is the TRL. The TRL is a measurement system developed by NASA used to assess the maturity level of a particular technology and can be summarized in figure 2-6.

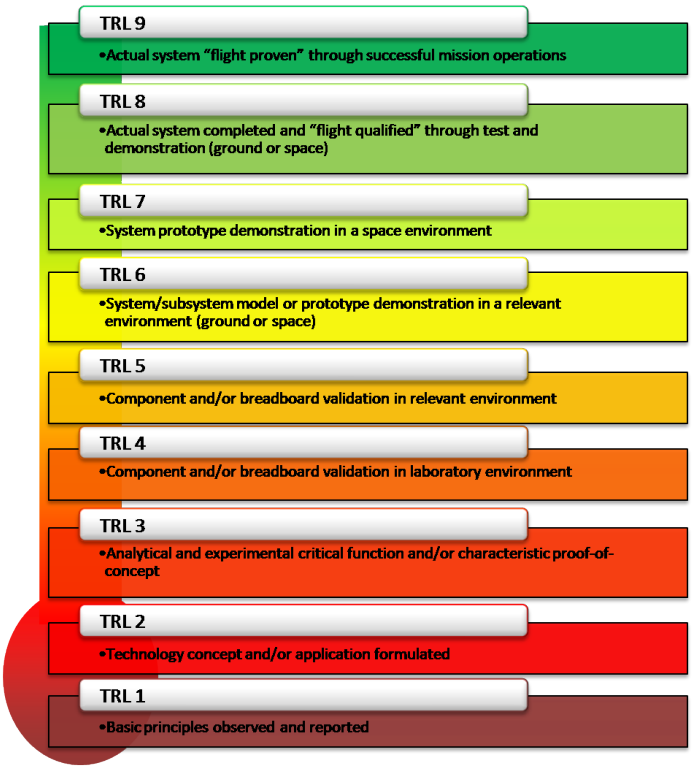

Figure 2-6: The TRL measurement system developed by NASA [41]

.

With the dimensions established, the comparison of the three solar tower CSP variants follows: The Gen3 variant is more efficient by several points compared to the

Variant	Cycle efficiency	TRL	Comments
Gen1	40.0%	TRL 7-9	Based on installations like Ivanpah [47]
Gen2	40.9%	TRL 7-9	Based on installations like Crescent Dunes [28]
Gen3	47.7%	TRL 5-7	Based on the Sandia G3P3 project [37]

Table 2.1: Efficiency and TRL for the three solar tower CSP variants

Gen1 and Gen2 variants. However, the Gen1 and Gen2 variants have already been

implemented commercially, but the Gen3 variant is still in a pilot plant testing and de-risking mode at this time. So far, the approach taken with the Gen1 and Gen2 solar tower CSP variants has been to build large, utility-scale installations, such as Ivanpah and Crescent Dunes in the US and more recently Shouhang Yumen, Power China Qinghai Gonghe, and SUPCON Delingha [17] all within the last couple of years in China. The question of whether the Gen3 variant should be built large or built modular will be explored in this work.

2.3 Literature about modeling a Gen3 solar tower CSP system

A Gen3 solar tower CSP plant is composed of the following components, as shown in figure 2-7. The components are as follows:

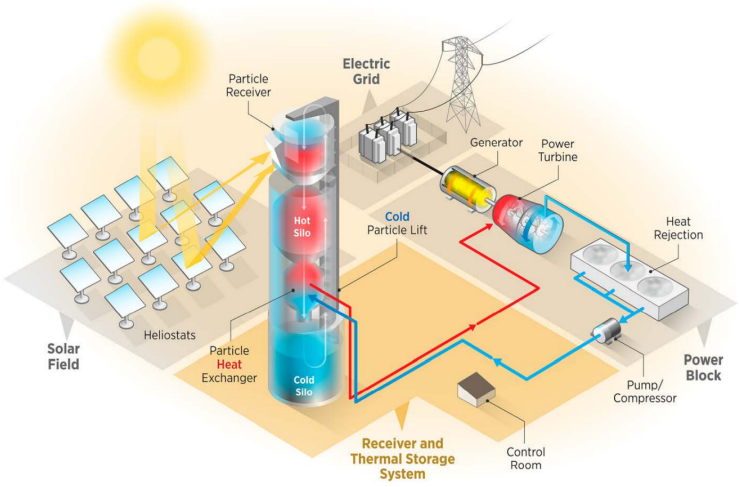

Figure 2-7: A schematic showing the major components of a Gen3 CSP plant [29]
.

- Solar (or heliostat) field - composed of multiple heliostats. The heliostats are mirrors that are mechanically actuated to track the sun to reflect and focus the solar energy on each mirror onto a small area (the receiver) at the top of the tower.

- Particle receiver - the particle receiver is what the heliostats are aiming at. The

function of this component is to transfer the focused solar energy coming from the heliostats to the heat transfer fluid, which are particles in a Gen3 solar tower CSP plant.

- Particle loop (within the tower) - the particle loop is composed of the hot silo, the cold silo, the particle side of the particle heat exchanger, and a cold particle lift. After being heated in the particle receiver, the particles fall into the hot silo where they are either stored for future use, immediately sent to the particle heat exchanger, or a combination of both. In the particle side of the particle heat exchanger, the particles transfer heat to the power generation block, which has its own heat transfer medium. After leaving the particle heat exchanger, the cooled particles are collected in a cold silo. To close the cycle, a cold particle lift vertically lifts the cooled particles up to the top of the tower where they can enter the receiver and the particle loop is complete.

- Power generation block - the power generation block is composed of the other half of the particle heat exchanger and a thermodynamic cycle that is capable of converting the thermal energy coming from the particles into electrical energy. The cycle of particular interest in this work is a closed Brayton cycle using sCO_2 as the heat transfer medium. In its most simple form, the closed Brayton sCO_2 cycle has the following components, however there are more complex forms that are covered later.

  - Turbine - the turbine expands hot sCO_2 exiting the particle heat exchanger, generating shaft work to power a generator which produces electricity for the grid and drives the compressor.
  - Heat rejection - heat from the low pressure sCO_2 exiting the turbine is rejected to atmosphere to reduce the volumetric flow into the compressor.
  - Compressor - the compressor compresses the cool, low pressure sCO_2 into high pressure sCO_2.
  - sCO_2 side of the particle heat exchanger - the high pressure sCO_2 is heated

before flowing into the turbine.

In order to build a model of a Gen3 solar tower CSP plant in Modelon Impact that can estimate the power generated by the plant at any given time during the year for use in a financial analysis based on performance, the following data is necessary for the approach used in this work:

1. Data to parameterize the components in the plant, including the components listed above

2. Data to estimate the costs of the components, to be summed into a total plant cost

3. Data to perform a financial analysis of a particular plant configuration

Each of these is addressed in the following subsections.

2.3.1 Data to parameterize the components in the plant

This section includes the data that was referenced to build the model of the Gen3 solar tower CSP plants in Modelon Impact. If a component is not mentioned here, then there were assumptions created to model that component and those will be covered in the Methodology section of this work.

Sun

A sun model is necessary to understand the behavior of the solar energy supplied to the plant. At the level of fidelity used for this work, there are three outputs needed from the sun model: DNI, azimuth, and elevation. The DNI value is the total solar energy per unit area available at a given time and a given location, while the azimuth and elevation are used to calculate the efficiency of the heliostat field. DNI data for locations in the US can be downloaded from the NSRDB via NREL's SAM software [33]. Sun azimuth (az) and elevation (el) for a given latitude are obtained through equations provided in [11] in the sun component in Modelon Impact.

Heliostat field

The heliostat field model takes solar azimuth and elevation from the sun model as an input and returns field efficiency. A rigorous heliostat field model was out of scope for this work. Rather, the heliostat field model uses the characteristics of the heliostat field described in [14] in the heliostat field component in Modelon Impact. In this

0	0	0.0873	0.2618	0.4363	0.7854	1.1345	1.5621
0	0	0.3014	0.5087	0.6195	0.6886	0.7052	0.7184
0.5236	0	0.3014	0.5075	0.6159	0.6862	0.7029	0.7184
1.0472	0	0.2931	0.4968	0.6052	0.6778	0.6993	0.7184
1.309	0	0.3348	0.5003	0.6016	0.6719	0.6957	0.7184
1.5708	0	0.2776	0.4813	0.5909	0.6671	0.6933	0.7184
1.9199	0	0.3181	0.4825	0.5849	0.66	0.6886	0.7184
2.2689	0	0.3228	0.4765	0.579	0.6952	0.685	0.7184

Table 2.2: Heliostat field efficiency from azimuth and elevation

table, the efficiency values are looked up (or interpolated) from the azimuth and the elevation. The azimuth values are in the first column and the elevation values are in the first row.

Receiver

An assumption for the annual efficiency of a particle receiver for a Gen3 solar tower CSP plant is provided in [21].

sCO_2 power generation block

Power generation blocks based on sCO_2 as the working fluid have the potential to yield higher thermal efficiencies at lower capital cost than state-of-the-art steam-based power cycles [16]. Compared to steam, sCO_2 has a higher energy density at typical operating conditions. The required volumetric flowrate of the working fluid is lower for sCO_2 than it is for steam, which reduces the size and cost of equipment required for a sCO_2 cycle compared to a steam cycle. The magnitude of the size difference involved can be visualized in figure 2-8. There are many different variants of sCO_2

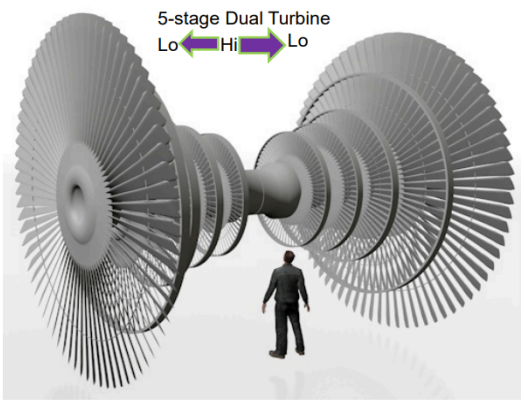

(a) The size of a 300 $MW_{(e)}$ steam turbine compared to a person [34]

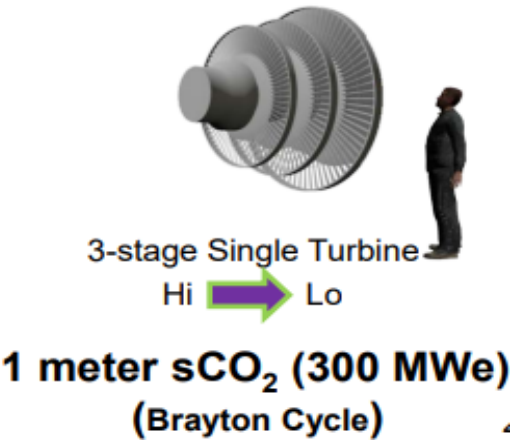

(b) The size of a 300 $MW_{(e)}$ sCO_2 turbine compared to a person [34]

Figure 2-8: At the same power delivered, the sCO_2 turbine is much smaller than the steam turbine

cycles, which generally trade complexity with efficiency. In this work, two cycles were chosen for simulation: Both are Brayton cycles. The recuperated cycle is less

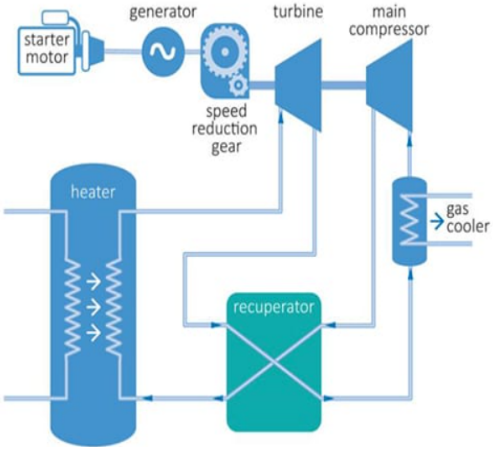

(a) A recuperated sCO_2 cycle [51]

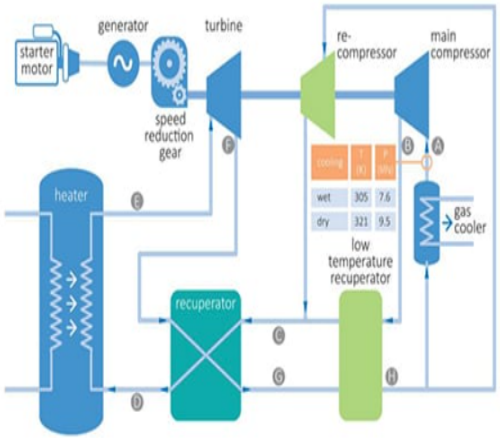

(b) A recompression sCO_2 cycle [51]

Figure 2-9: Layouts of two different types of sCO_2 cycles

complex than the recompression cycle, since it only has a single recuperator, main compressor and a turbine. The recompression cycle has an additional recuperator and a recompressor. By virtue of having less equipment, the recuperated cycle is less expensive than the recompression cycle, but the recuperated cycle is also less efficient than the recompression cycle.

Although there are more complex sCO_2 cycles in development, these two variants were selected because they have the lowest LCOE per Heller et al [21]. In the same study, Heller et al also describe optimum parameters for sCO_2 cycles, including turbine inlet pressure, compressor inlet pressure, heat exchanger performance (heat transfer and pressure drops), and recompression fraction (for the recompression cycle only). For a cycle efficiency between 37% and 42%, the LCOE is lowest for turbine inlet temperatures of 550°C. The only remaining parameter to be specified is the optimum compressor inlet temperature, which is assumed to be 32°C for a wet-cooled system per Dyreby et al [12].

In addition to the modeling the design point, it is also necessary to model off-design points as the available heat input to the sCO_2 cycle from a Gen3 solar tower CSP plant varies hourly. Dyreby provides a methodology for modeling the behavior of turbomachinery at design and off-design points for a 10 MW_e sCO_2 Brayton cycle [13]. The implementation of these models is discussed in the Methodology section.

2.3.2 Data to estimate the cost of components in the plant

The following table summarizes the correlations used to estimate the cost of each component to roll up into a total plant cost. Cost correlations exist for each of the

Component	Cost formula	Units of x	Validity range of x	Source	Comments
Heliostat field	$160 * x$	m^2	NS	[33]	-
Tower incl. vert transport	$560,000 + 913 * x^{1.66}$	m	NS	[21]	-
Receiver	$33 * x$	kW_{th}	NS	[21]	-
Particle inventory	$1.1 * x$	kg	NS	[21]	-
TES system	$6.27 * x$	kW_{th}	NS	[21]	-
Particle HX	$3,266 * x^{0.66}$	W_{th}/K	NS	[21] [6]	$T_{max} \leq 550°C$
Recuperator	$49.45 * x^{0.7544}$	W_{th}/K	1.6e5-2.15e8 W/K	[45]	-
Cooler	$32.88 * x^{0.75}$	W_{th}/K	8.6e5-7.5e7 W/K	[45]	-
Turbine (radial)	$406,200 * x^{0.8}$	MW_s	8-35	[45]	$T_{max} \leq 550°C$
Turbine (axial)	$182,600 * x^{0.5561}$	MW_s	10-750	[45]	$T_{max} \leq 550°C$
Compressor (centrifugal)	$1,230,000 * x^{0.3992}$	MW_s	1.5-200	[45]	-
Motor (open drip-proof)	$399,400 * x^{0.6062}$	MW_e	0.00075-37	[45]	-
Generator	$108,900 * x^{0.5463}$	MW_e	4-750	[45]	-
Piping and valves	$0.15 * x$	Power block cost ($)	NS	[20]	-

Table 2.3: Cost correlations for Gen3 solar tower CSP plant components

major components in the Gen3 solar tower CSP plant, allowing for an estimate of the total cost of the plant once the costs are rolled up. Note that the power block

equipment costs are provided as equipment-only costs, while the other equipment costs are total installed costs. However, there is only a limited number of sources to corroborate these values, which isn't surprising given that the Gen3 solar tower CSP concept is at a low TRL relative to Gen1, Gen2, or the other CSP plant designs. Notably, Heller et al refer to power block costs from a simulation tool provided by STEAG Energy Services GmbH, but these costs are confidential and could not be used in this work [21].

Combined with the fact that there isn't a validity range for all of the component cost correlations, this implies that there is a high level of uncertainty in the total cost of the plant. Weiland et al provide an uncertainty range of -28% to +35% for the cost of a 10 MW_e plant. However, given that costs of components and equipment are usually higher rather than lower, especially for low TRL equipment, it seems optimistic to assume that a cost of -25% of the reference value is nearly equally as likely as +25%. The assumption for uncertainty in this work is covered in the Methodology section.

2.3.3 Data to perform a financial analysis of a particular plant configuration

There are three parameters in the financial analysis used for the NPV calculation that are independent of the location of the plant or the size of the plant:

- Discount rate
- Yearly operating costs
- Learning rate

A discount rate assumption of 9% can be found in NREL's SAM [33] for Gen2 solar tower CSP plants. Given that discount rates are inherently subjective, this seems to be a reasonable starting assumption for Gen3 solar tower CSP plants. Yearly operating costs are estimated to be 2% of the installed capital for Gen3 solar tower CSP plants per [21], which also seems to be a reasonable starting assumption.

The learning rate describes how the cost of the nth unit relates to the cost of the first unit. In this form, the expression for the cost of the nth unit follows the functional relationship proposed by Wright which describes how the cost of the nth unit is a function of the cumulative production up to the nth unit [49].

$$y = ax^b$$

Where y is the cumulative average cost per unit, x is the cumulative number of units produced, a is the cost of the first unit, and b is a function of the learning rate.

Since the learning rate is only meaningful when there are multiple units, it applies only in the modular build approach, where many Gen3 solar tower CSP plant modules are built over time rather than one single large Gen3 solar tower CSP plant (which wouldn't benefit from a learning rate).

Given that the Gen3 variant is at a low TRL, the learning rate warrants some additional scrutiny. First, to define the learning rate, LR, as it relates to the progress ratio, PR:

$$LR = 1 - PR$$

Then the cost of the nth unit is:

$$c_n = c_1 * (\frac{n}{1})^{\frac{logPR}{log2}}$$

Where c_n is the cost of the nth unit, c_1 is the cost of the first unit and n is the number of the nth unit.

For CSP, there are multiple sources stating that the learning rate LR is between 10-12% [5] [30] [23] [42] [24] [36]. This is typically portrayed in comparison to solar PV, which has studied extensively and a learning rate in the low 20s% has been corroborated by multiple sources [5] [40]. Therefore, one could conclude that CSP doesn't show as much potential as solar PV to reduce costs quickly over time in the race to supplant conventional hydrocarbon-based sources of energy.

However, there is reason to doubt this conclusion. First, solar PV has been archi-

tecturally stable for many decades, while CSP has not. There are not only different forms of CSP (solar tower, parabolic trough, etc.) but also different variants of these forms as well (e.g. Gen1, Gen2, etc.). Due to the ubiquity of solar PV in recent years, there is a lot of data on the performance of solar PV from the utility to the residential scale, and since solar PV has been architecturally stable, it is straightforward to directly compare iterations of solar PV over time. However, CSP has not grown in capacity like solar PV, as per figure 2-1. The data set on CSP as a whole is therefore limited compared to PV, and the data set is even further limited once the different types of CSP are taken into account as per figure 2-1. It does not seem reasonable to compare cost data of a parabolic trough installation with no thermal storage with the cost of a power tower with thermal storage. Lastly, since there is more interest in solar PV than CSP, the learning rate of CSP is not covered in academic work as heavily as solar PV. These references [30] [23] [42] [24] [36] where the learning rate of CSP is quoted in the relatively tight range of 10-12% are at minimum 7 years old at the time of this writing.

All of this implies there is high uncertainty in the learning rate of CSP as a whole, especially when considering a particular variant such as a Gen3 solar tower CSP plant that has a low TRL and there is not enough data available on it to fix a learning rate to a tight range. Lilliestam et al explore CSP learning rates in [26] but do not draw any conclusions for solar tower technology. Using capital cost data from IRENA as shown in figure 2-5 [1], different estimates of the learning rate can be obtained in figure 2-10. When considering the data set includes all forms of CSP (parabolic trough, solar tower, linear fresnel), all with varying amounts of storage, then the data could be filtered to just look at power tower applications with 10+ hours of thermal storage in figure 2-11. The points shown are mainly Gen2 (molten salt) solar tower CSP plants that have been built in China in recent years. Although there are only 3 data points and it might seem foolish to draw a conclusion about the learning rate from this limited set of data, these 3 data points represent the closest analog to a Gen3 solar tower CSP plant.

The concluding point is that there is significant uncertainty in the learning rate of

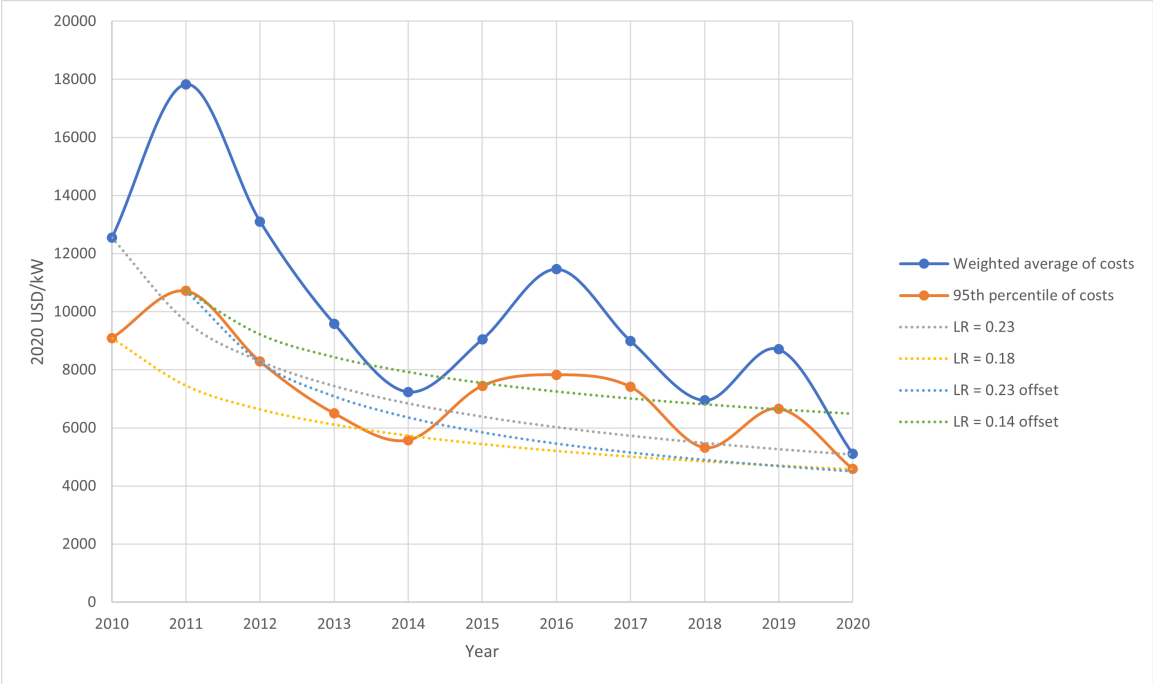

Figure 2-10: None of the lines fits the data exactly, but it appears that the learning rate could be anywhere between 0.14 and 0.23 in this data set from [1].

CSP. It could be as low as 10%, as per most of academic literature, or it could be up to 30%, or somewhere in between. Until there is a preponderance of data available on the learning rate of Gen3 solar tower CSP plants, the actual learning rate realized by a firm in the CSP market will depend on the approach they take to CSP.

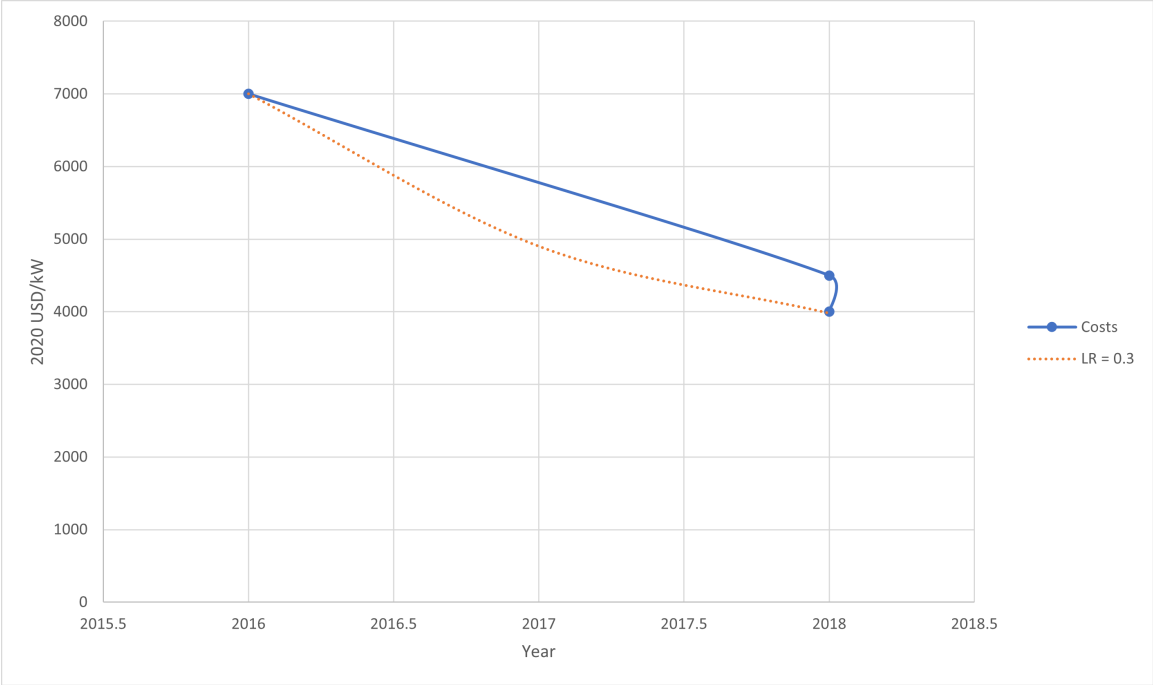

Figure 2-11: When filtered for Gen2+ CSP, the data set from [1] is much smaller, and the learning rate that matches the start and the end is 0.3.

Chapter 3

Methodology

A 5-step process for comparing the viability of a "build large" approach with a "build modular" approach for a Gen3 solar tower CSP installation is described in this chapter.

1. Definition of plant sizes, locations, and capacity factors used for both approaches.
2. Plant model implementation for both approaches in Modelon Impact.
3. Cost estimates of both approaches in Excel.
4. NPV calculation in Excel for both approaches using deterministic inputs.
5. NPV calculation in Excel for both approaches using stochastic inputs for specified variables.

3.1 Definition of plant sizes, locations, and capacity factors used for both approaches

The "build large" approach was assumed to be a single 100 MW_e plant. This is similar to the 110 MW_e nominal capacity of the most recent CSP plant in the United States, a Gen2 solar tower plant with thermal storage called the Crescent Dunes Solar

Energy Project [46]. It also matches the nominal capacity of Gen2 solar tower CSP plants with thermal storage recently being built in China - the Shouhang Yumen 100 MW Tower CSP Project and the Shouhang Dunhuan Phase II - 100 MW Tower CSP Project, which are both under construction as of December 5, 2021. [17]. For the "build modular" approach, the module size was assumed to be 1/10th of the 100 MW_e plant used for the "build large" approach, or 10 MW_e. This matches the nominal capacity of the sCO_2 cycle that Dyreby created nondimensional turbomachinery maps for [13]. It also matches the capacity of the Gen2 solar tower CSP project Solar Two that was the precursor to the commercial Gen2 implementations.

Three locations of interest were chosen to perform the evaluation, as follows:

- Daggett CA is in the Mojave Desert in southern California. It is in the region that has the highest solar irradiance in the United States and is close to Los Angeles county, a large population center. It has a desert climate.

- New Orleans LA is in an area of the United States where there is a lot of industry (chemical plants, refineries, etc.) with hard-to-abate CO_2 emissions. It is in a subtropical climate zone.

- Boston MA is in a major population center in the United States. It is in a temperature climate zone.

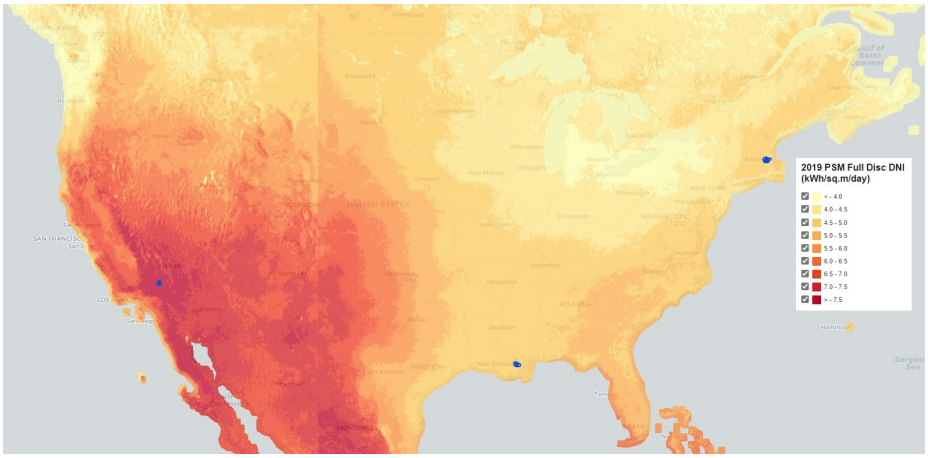

Figure 3-1: The three approximate locations of interest. Data from the NSRDB data viewer with the 2019 PSM Full Disc DNI data overlaid. [32]

Lastly, three different capacity factors were chosen. The capacity factor is a dimensionless quantity that is an important metric for renewable power technologies. It describes the ratio of the actual power produced by a system over a chosen time period divided by the power that would have been produced by the system if it was operating at maximum capacity continuously for the same time period.
The three capacity factors chosen were 20%, 30%, and 40%. Their significance is as follows:

- 20% CF is currently at the upper edge of what solar PV can deliver, per figure 3-2.

- 30% CF is what Ivanpah, a Gen1 solar tower CSP plant, was originally designed to deliver [4].

- 40% CF is what current Gen2 solar tower CSP plants are targeting, per figure 3-2.

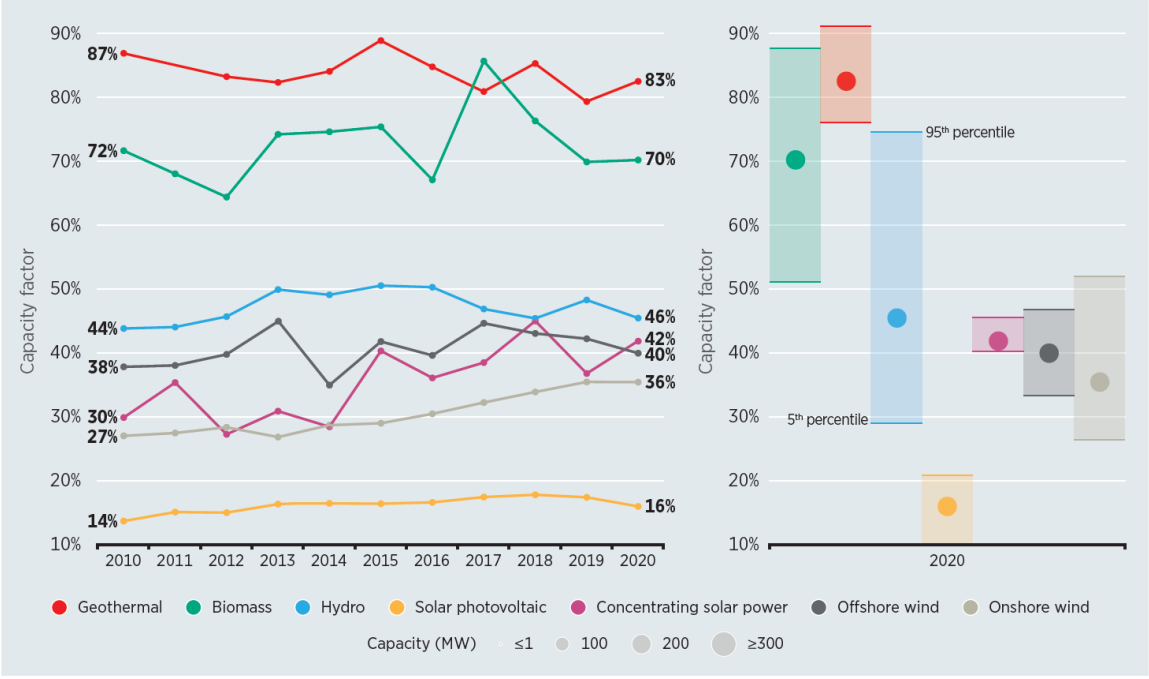

Source: IRENA Renewable Cost Database

Figure 3-2: Global weighted-average utility-scale capacity factors by technology, 2010-2020 [1]

The following table shows how these three capacity factors correspond to annual electricity production:

Capacity factor	10 MW_e plant	100 MW_e plant
20%	17,520 MWh/year	175,200 MWh/year
30%	26,280 MWh/year	262,800 MWh/year
40%	35,040 MWh/year	350,400 MWh/year

Table 3.1: Different capacity factors applied to 10 MW_e and 100 MW_e plants

3.2 Plant model implementation for both approaches in Modelon Impact

In this section, the implementation for each of the components in the 10 MW_e and 100 MW_e plants in Modelon Impact is described.

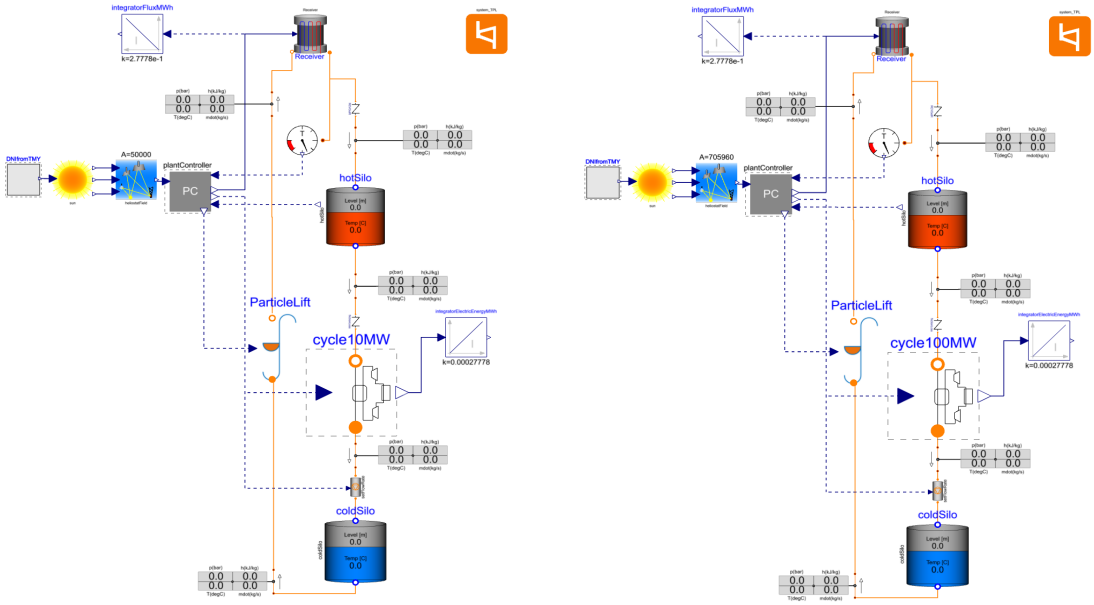

(a) 10 MW_e plant in Modelon Impact (b) 100 MW_e plant in Modelon Impact

Figure 3-3: At a high level, the architecture of both plants is similar. The differences lie in the parameterization of the components.

3.2.1 DNI input to the Sun model

The DNI input is a table of 8,760 rows (the number of hours in a year) corresponding to the DNI data in the TMY data file for the selected location. There is a separate TMY file for each location (Daggett, New Orleans, Boston). The TMY data comes from the NSRDB via NREL's SAM tool [33]. The table is configured to interpolate using a modified Akima spline which ensures the first derivative of the DNI is continuous. A plot of the data is shown in figure 3-4. The trends are "spiky", which is expected because the sun rises and sets every day.

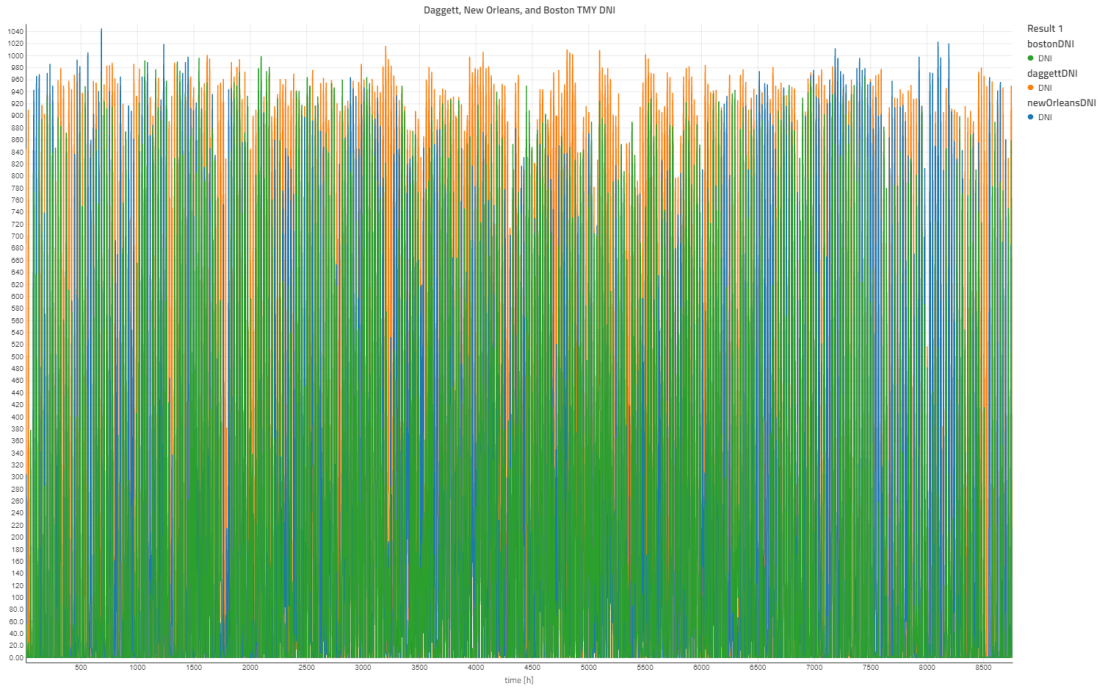

Figure 3-4: The TMY DNI for Daggett is consistently high, but there are times when the DNI for New Orleans is higher, especially in the early and late months. As expected, the DNI for Boston is lower than the others [33]

3.2.2 Sun model

The sun model is a component that comes with Modelon Impact. Given a latitude, it can return DNI, azimuth and elevation based on the "clear sky" model documented by Duffie and Beckman [11]. However, for this plant model, the calculated DNI output feature is turned off and it uses the DNI coming from the selected location-specific

TMY data file instead. The azimuth and elevation are still calculated, and along with the "pass-through" DNI input from the TMY data file, are passed to the heliostat field block. The latitudes used as input into the azimuth and elevation calculation are shown in the following table:

Location	Latitude input to Sun model
Daggett, CA	34.6853 deg
New Orleans, LA	29.9506 deg
Boston, MA	42.3589 deg

Table 3.2: Latitudes of the three different locations referenced in this work

3.2.3 Heliostat field

The heliostat field is also a component that comes with Modelon Impact. It has a 2D matrix that looks up an interpolated efficiency given the azimuth and elevation outputs from the preceding sun model. The 2D matrix used comes from Ehrhart and Gill [14] and is described in this work in section 2.3.1. Three mirror-specific parameters are as follows:

- Mirror reflectivity - 0.9
- Mirror cleanliness - 0.95
- Mirror absorptivity - 0.94

Each of these factors serves to moderate the total power delivered to the receiver, as expected. For example, a mirror that is not completely clean will not deliver as much power to the receiver as a clean mirror if all other parameters are equal.
The last parameter is the area of the heliostat field in m^2. These are determined by manual iteration - once the system model is complete, the heliostat field area is adjusted until the system delivers the desired power for a given location. A table of the heliostat field areas used for the 10 MW_e plant is as follows: For the 100 MW_e plant, the same table is as follows: The trends for each location versus capacity factor can also be visualized in a graph:

10 MW_e plant location	20% CF	30% CF	40% CF
Daggett, CA	55,000 m^2	77,000 m^2	100,000 m^2
New Orleans, LA	83,000 m^2	117,000 m^2	186,000 m^2
Boston, MA	90,000 m^2	135,000 m^2	235,000 m^2

Table 3.3: 10 MW_e plant required heliostat areas by location

100 MW_e plant location	20% CF	30% CF	40% CF
Daggett, CA	510,0000 m^2	706,000 m^2	900,000 m^2
New Orleans, LA	770,000 m^2	1,060,000 m^2	1,510,000 m^2
Boston, MA	845,000 m^2	1,197,500 m^2	1,830,000 m^2

Table 3.4: 10 MW_e plant required heliostat areas by location

(a) 10 MW_e plant required heliostat areas by location

(b) 100 MW_e plant required heliostat areas by location

Figure 3-5: The required heliostat area is lowest and generally linear against CF in Daggett for both plants. The required heliostat areas for New Orleans and Boston are higher and show superlinearity against CF especially at the higher CFs.

3.2.4 Receiver

The receiver is a custom component built for this work in Modelon Impact. It consists of a pseudoreceiver whose efficiency is not calculated rigorously, but rather uses a fixed constant value of 86.7% as assumed by Heller et al [21] as the annual average efficiency of a receiver. No other dynamics are modeled.

3.2.5 Hot Silo and Cold Silo

The hot silo and cold silos are components that come with Modelon Impact. The heat transfer parameterization for both silos is the same across all cases and as follows:

- Total thermal resistance of the tank wall - 20,000 K/W
- Specific heat of the tank wall - 1060 J/(kg-K)

The silo dimensions are the same between the hot silo and the cold silo but vary with the type of plant - 10 MW_e or 100 MW_e. The rules of thumb used to parameterize the silos are as follows:

- The hot silo has the same dimension as the cold silo.
- The silo diameter is half of the silo height.
- The maximum working inventory of the silo is 80% of the total volume.
- The silos are sized to hold 16 hours of particle flow at the turndown flow rate through the power block (the turndown flow rate is described in detail in in the power block subsection). The intent behind this rule of thumb was to design the plant such that it was capable of delivering power for a 16 hour night if the hot silo was filled to the maximum working inventory during the daytime while the sun was out.

After applying the assumptions below, the silos were sized as follows:

- 10 MW_e
  - Height - 16.3 m
  - Diameter - 8.15 m
- 100 MW_e
  - Height - 38.2 m
  - Diameter - 19.1 m

Finally, the silos were set to initialize with the hot silo virtually empty and the cold silo at 90% of its total volume.

3.2.6 Particle Lift

The particle lift is a custom component built for this work in Modelon Impact. It consists of an idealized flow controller that takes input from the plant master control block. One of the functions of the plant master control block (described in full in a later subsection) is to control the flow rate between the cold silo and the hot silo through the receiver, and the particle lift component is what implements the signal from the plant master control block.

The power requirements and the heat loss for the particle lift are not modeled. Both are assumed to be negligible.

3.2.7 Particle Medium

The particle medium does not appear directly on the flowsheet, but it is present in all of the components that see particle flow. In this work, the particles are assumed to be a particular type called CARBO HSP 40/70 and modeled as a pseudofluid, so fluid properties like flow regimes or frictional losses are not modeled. Instead, the only two properties that are modeled are specific heat as a function of temperature (see figure 3-6) and thermal conductivity as a function of temperature (see figure 3-7). The density of the particle pseudofluid is assumed to be constant at 2125 kg/m^3.

3.2.8 sCO_2 Power Block

Implementation in the plant model

The sCO_2 block representation on the plant model level is a custom component built for this work. On the holistic plant model level, the representation of the sCO_2 power block is a simple lookup table calculation. This approach was chosen to minimize the runtime of the plant model while still capturing the important dynamics of the

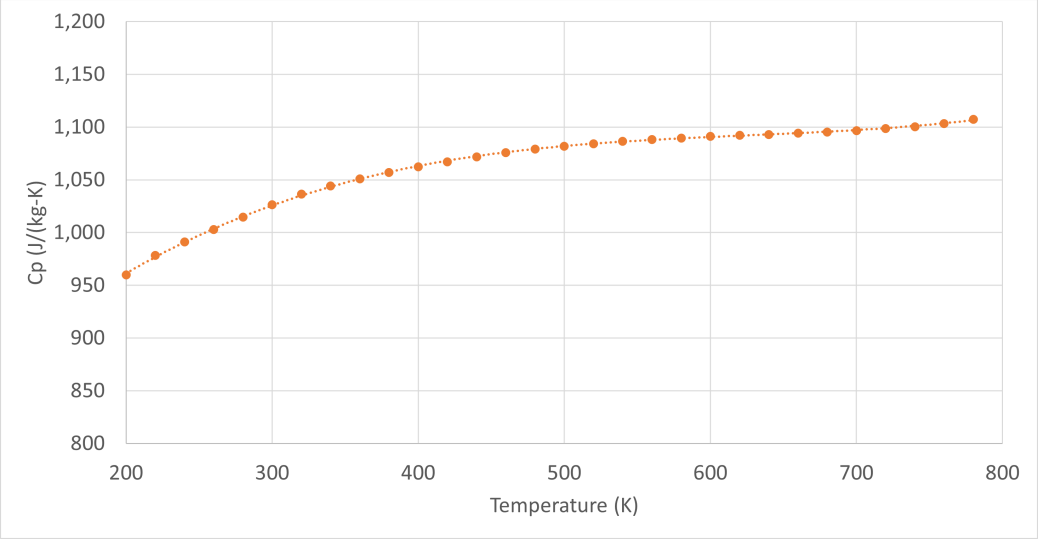

Figure 3-6: Specific heat of CARBO HSP 40/70 by Georgia Tech [39]

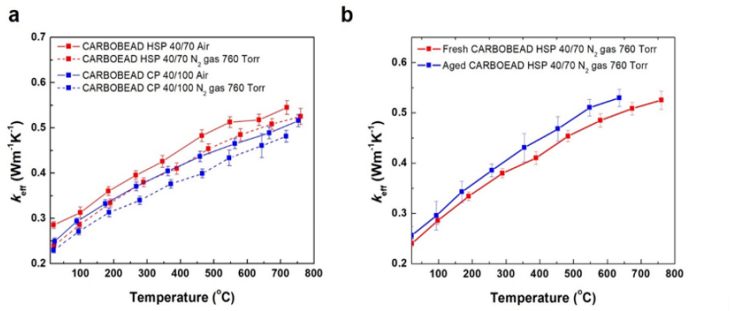

Figure 4 (a) Effective thermal conductivity as a function of temperature for CARBOBEAD HSP 40/70 and CARBOBEAD CP 40/100 in air and N_2 gas at 760 Torr; **(b)** Effective thermal conductivity as a function of temperature for fresh and aged HSP 40/70 under N_2 gas at 760 Torr.

Figure 3-7: Thermal conductivity of CARBO HSP 40/70 by Chung et al [7]

sCO_2 power block - namely, operational turndown limits, particle exit temperature, and cycle efficiency as a function of particle flow rate. The lookup value for the table is the particle flowrate, and the table returns an interpolated cycle efficiency. The power block component also calculates the total power generated using the particle flow rate, the particle inlet temperature, and the cycle efficiency. The power generated is integrated across the entire simulation timespan to return the cumulative MWh of electricity generated.

A schematic of the sCO_2 power block representation in the plant model is shown in figure 3-8. There are two cycle tables - one for the 10 MW_e plant and one for the

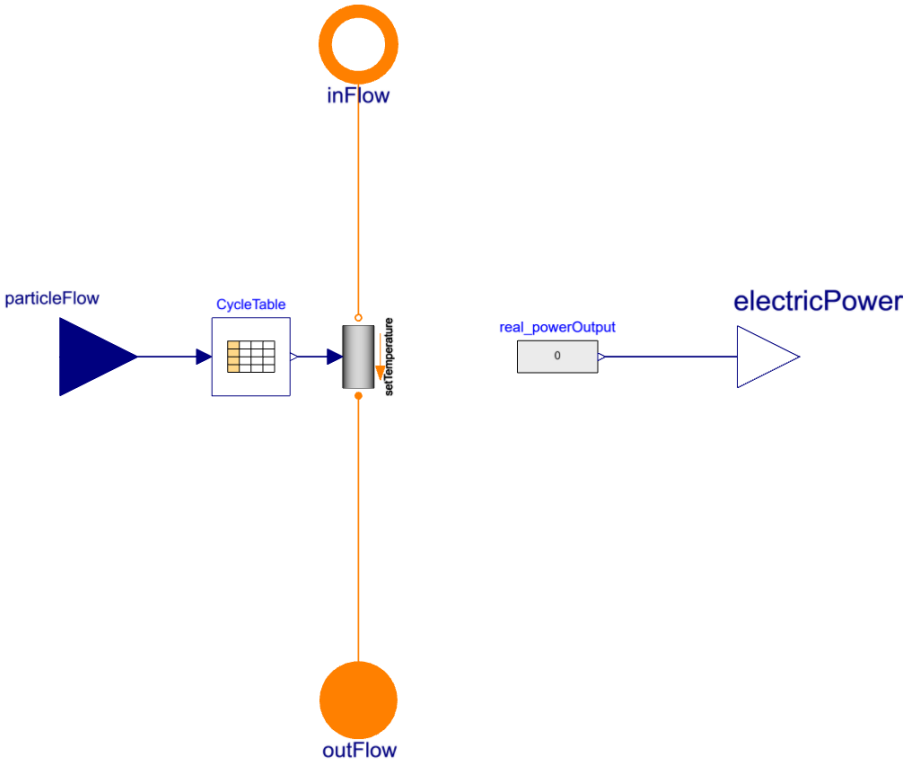

Figure 3-8: The representation of the sCO_2 power block at the plant model level is a simple lookup table

100 MW_e plant. The cycle table for the 10 MW_e plant follows:

Particle flow (kg/s)	Cycle efficiency (%)	Particle exit temperature (°C)	Corresponding power (MW)
0	0	194.5	-
25	0	194.5	-
25.1	27.1	194.5	4
30.1	29.6	219.6	5
35.3	31.7	244.8	6
41	33.5	271	7
47.5	35.0	299.2	8
55.1	36.4	330	9
64.2	37.6	363.9	10

Table 3.5: Cycle efficiency, particle exit temperature, and power generated vs particle flow for the 10 MW_e cycle

The cycle table for the 100 MW_e plant follows, which has an added dimension of recompression flow fraction due to the choice of the cycle modeled. The efficiency of both cycles across their range of operations is juxtaposed in figure 3-9.

One feature of the sCO_2 lookup table approach is the ability to manually force the cy-

Particle flow (kg/s)	Cycle efficiency (%)	Particle exit temperature (°C)	Corresponding power (MW)	Recompression fraction
0	0	282.3	-	-
323.3	0	282.3	-	-
323.4	31.1	282.3	50	0.374
386	33.0	308.6	60	0.368
455.9	34.7	336.1	70	0.363
538.5	36.1	365.8	80	0.358
636.4	37.3	397.5	90	0.353
752.9	38.6	430.4	100	0.350

Table 3.6: Cycle efficiency, particle exit temperature, recompression fraction and power generated vs particle flow for the 100 MW_e cycle

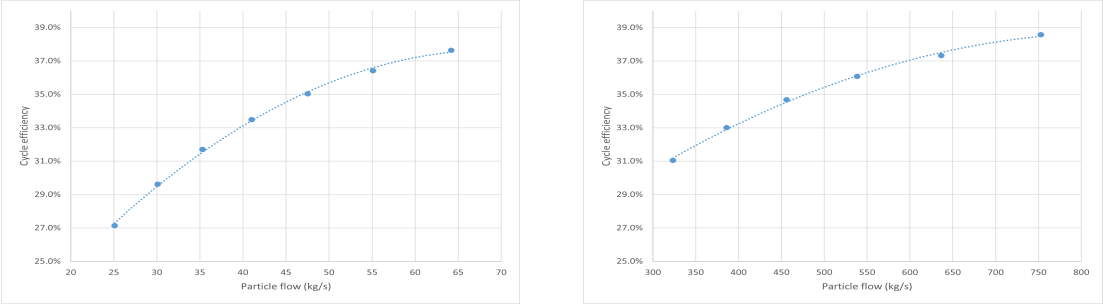

(a) 10 MW_e cycle efficiency vs particle flow rate

(b) 100 MW_e cycle efficiency vs particle flow rate

Figure 3-9: Cycle efficiency across the range of particle flow rates for both cycles

cle efficiency to zero when the power goes below the assumed minimum turndown. If the sCO_2 cycle was fully represented in the plant model rather than as an abstraction, the simulation stability and runtime would suffer when the heat input stopped to the sCO_2 cycle at night because the sCO_2 pressures and temperatures could transition between the supercritical regime and other regimes. This is not realistic for a real Gen3 solar tower CSP plant which would likely shut the sCO_2 cycle down rather than attempt to keep it running, but this implementation of the system model does not allow for the ability to shut down and start up the cycle. For the 10 MW_e cycle, the minimum electrical power production is assumed to be 4 MW_e (40% of the rated electrical power production), and for the 100 MW_e cycle, the minimum electrical power production is assumed to be 50 MW_e (50% of the rated electrical power production). The basis behind these numbers is covered in the following subsections.

Creating the lookup tables

The lookup tables are generated by independent models of the 10 MW_e and 100 MW_e sCO_2 cycles. These cycles are designed with the particle boundary conditions defined externally in the wrapper as shown in figure 3-10. The particle inlet temperature is

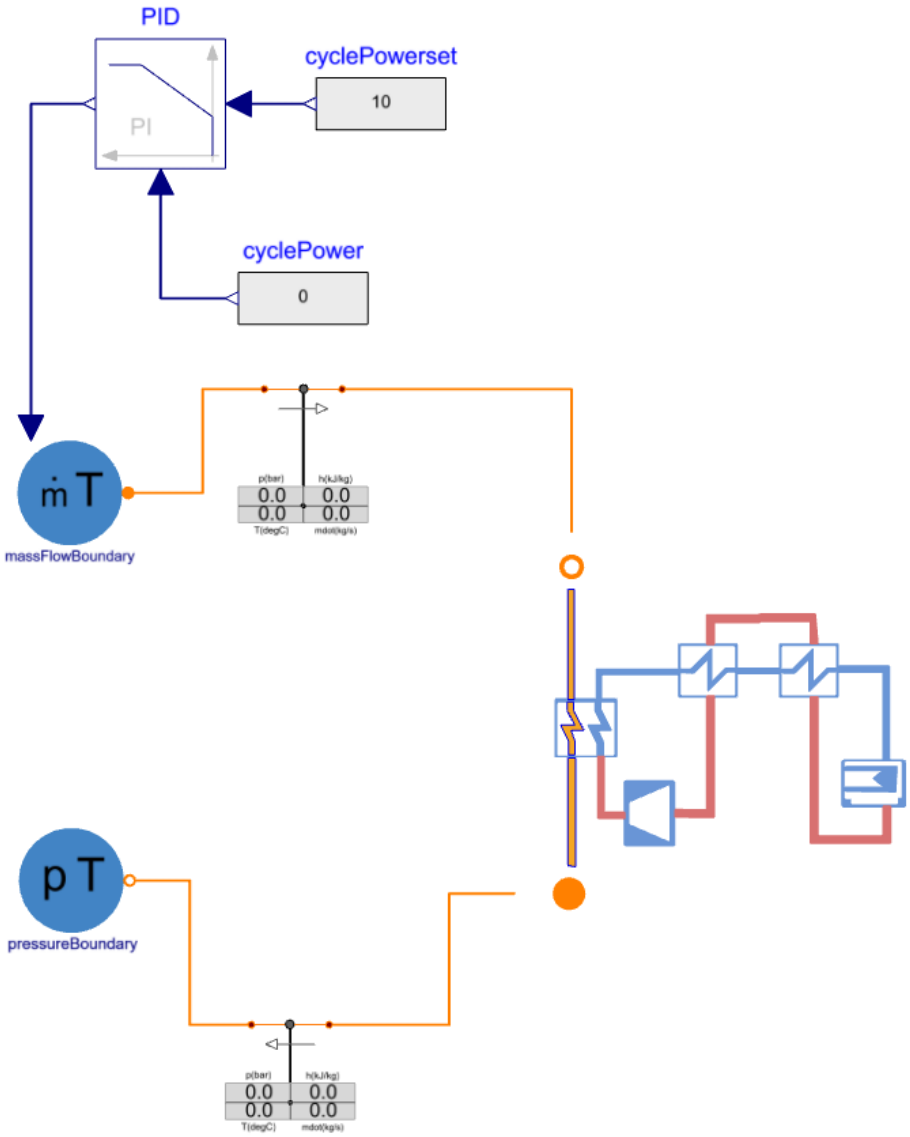

Figure 3-10: Wrapper for the sCO_2 cycle models that specifies the particle boundary conditions. The sCO_2 cycle model is the replaceable graphic on the right of the image above.

specified at a fixed 750 °C, the nominal temperature of the particles in the hot silo. The mass flow rate is set by a PID controller that receives the calculated net cycle power as an input and has a user-entered value for the setpoint. For example, for the

10 MW_e cycle, the setpoint corresponding to the design point would be 10. On the exit side, the particle outlet mass flow rate is fixed to be equal to the particle inlet mass flow rate due to the conservation of mass and the temperature is determined by the performance of the particle heat exchanger contained within the sCO_2 cycle model. Using this wrapper, the setpoints for the net cycle power can be varied to generate a table of particle mass flow rate and the corresponding values for particle exit temperature and cycle efficiency that are used in the sCO_2 lookup table.

The 10 MW_e sCO_2 cycle model

The 10 MW_e sCO_2 cycle, associated with the 10 MW_e "build modular" approach, was assumed to be the simple recuperated variant. The layout of the simple recuperated variant is shown in figure 2-9a. This cycle was chosen because it appears to have the lowest LCOE of the 10 variations studied by Heller et al, owing to its competitive efficiency with minimal capital requirements because it only has two main turbomachines and three heat exchangers [21]. Due to the simplicity of the cycle, it seemed to be well suited to the "build quick, cheap and efficient" approach espoused by the "build modular" approach. With the simple recuperated sCO_2 cycle variant selected,

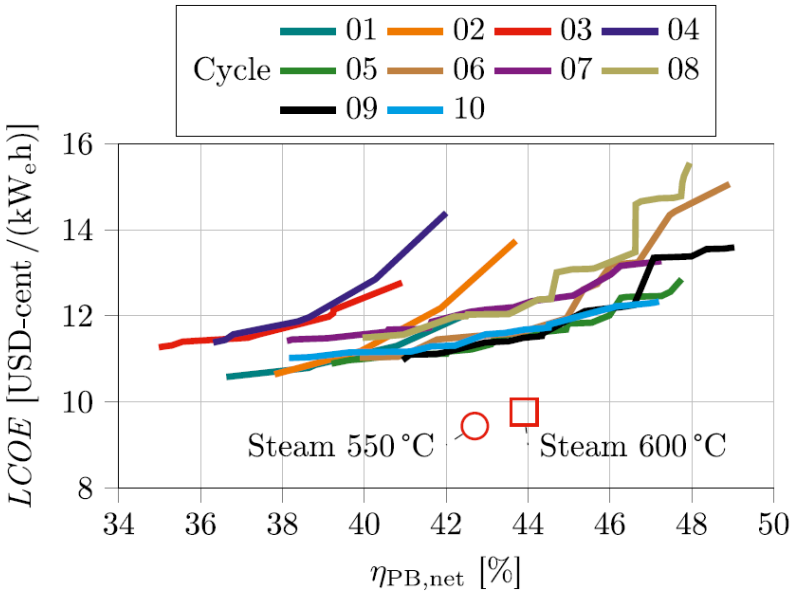

Figure 3-11: LCOE Pareto fronts of 10 different sCO_2 cycle variants. The simple recuperated variant is the "01" cycle, the recompression variant is the "05" cycle [21].

the medium specified for simulating the properties of CO_2 is the Span and Wagner EOS [38], a prebuilt component in Modelon Impact. Then, the pressure profile for the cycle and the exchanger performance is as follows:

- The turbine inlet pressure was assumed to be 260 bar per Heller et al [21].
- The TIT was assumed to be 550 °C per Heller et al. Although higher inlet temperatures were studied, the optimum TIT was determined to be 550 °C [21], Furthermore, the correlations for costing cycle equipment, particularly the particle heat exchanger, at TITs above °C were marked as confidential and were therefore unavailable for use.

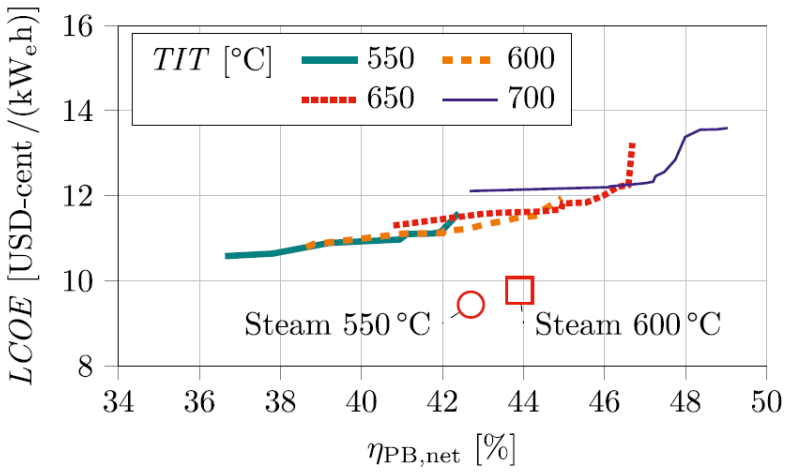

Figure 3-12: A TIT of 550 °C is Pareto optimal for a power block with a net efficiency between 36% and 42% [21]

.

- Exchanger pressure and heat transfer performance. Since heat exchanger geometry isn't known, the exchangers were designed using a eps-NTU approach where only the area is specified. The source for the assumptions is Heller et al [21] unless otherwise specified:
  - For the recuperator, the pressure drop on the high pressure pass was assumed to be 3% and 2% for the low pressure pass. It was sized to achieve a 10 °C TTD at the design point, corresponding to a heat transfer area of 158 m^2. The heat transfer coefficients on both sides (both sCO_2) were

automatically calculated using a Reynolds-based correlation prebuilt in Modelon Impact.

  - For the particle heat exchanger, the pressure drop on the sCO_2 pass was assumed to be 2%. It was sized to achieve a 50 °C TTD at the design point, corresponding to a heat transfer area of 920 m^2. The heat transfer coefficient on the sCO_2 pass was automatically calculated using a Reynolds-based correlation prebuilt in Modelon Impact. The particle heat transfer coefficient was assumed to be 300 $W/(m^2 - K)$ per Albrecht and Ho [3].
  - For the cooler, the pressure drop on the sCO_2 pass was assumed to be 0.6%. The cooler wasn't modeled rigorously as a heat exchanger in the cycle model for the purposes of simplicity, so the LMTD was assumed to be 7.2 °C with the hot end approach of 5 °C, and an air inlet temperature of a constant 22 °C.

- The compressor inlet pressure was assumed to be 75 bar.
- The compressor inlet temperature was assumed to be 32 °C per Dyreby et al [12].

The turbine and compressor were designed and parameterized using the following process:

1. The isentropic efficiency of the turbine was assumed to be a constant 0.91, and the efficiency of the connected generator was assumed to be 0.987 per [21]. Using these values and the cycle pressure profile (specifically turbine inlet pressure, TIT and turbine outlet pressure) specified above, the turbine outlet temperature and the power generated by the turbine+generator at varying mass flow rates through the turbine can be calculated.

2. The isentropic efficiency of the compressor was assumed to be 0.87 at the design point, and the efficiency of the connected motor was assumed to be 0.97 per [21]. Using these values and the cycle pressure profile (specifically compressor inlet pressure, compressor inlet temperature, and compressor outlet pressure)

specified above, the compressor outlet temperature and the power consumed by the compressor+motor at varying mass flow rates through the turbine can be calculated.

3. The mass flows through the turbine and compressor are set equal and the mass flow is manually iterated until the net power (the sum of the power generated by the turbine+generator and the power consumed by the compressor+motor) matches the design point, in this case 10 MW_e.

4. The compressor speed at design point is manually iterated to achieve a specific speed Ns of approximately 60 and a specific diameter Ds of 2.5 assuming that specific speed Ns is $\frac{speed*V^{0.5}}{h^{0.75}}$, the specific diameter Ds is $\frac{0.95*154}{Ns}$, and the compressor rotor diameter D is calculated as $\frac{Ds*V^{0.5}}{h^{0.25}}$ using the Ns-Ds methodology published by Nichols [31].

5. The compressor maps are built for 5 speed lines using the nondimensional methodology proposed by Dyreby [13], where ϕ^* is a function of mass flow rate, η is a function of isentropic efficiency, and ψ is a function of isentropic enthalpy rise:

$$\phi^* = \frac{\frac{m}{\rho\pi D^2/4}}{N\pi D\phi_{scale}}$$

$$\eta = (-0.7069+168.8\phi^*-8089(\phi^*)^2+182725*(\phi^*)^3-1638000(\phi^*)^4)*\eta_{max}/0.6838$$

$$\psi = (0.04049 + 54.7\phi^* - 2505(\phi^*)^2 + 53224(\phi^*)^3 - 498626(\phi^*)^4) * \psi_{max}/0.4816$$

ϕ_{scale} is goalseeked to set ensure the peak efficiency η is at the design point, and both η_{max} and ψ_{max} are goalseeked to match the desired outlet pressure and outlet temperature at the design point mass flow rate calculated in step 3. The map design process yields the following in figure 3-13:

With the turbomachinery parameterized, the entire cycle can now be modeled at the design point (10 MW_e) in figure 3-14. The final element of the cycle required to automatically resolve off-design points is the control system. The cycle control system uses a PID controller to reduce the speed of the compressor to control the

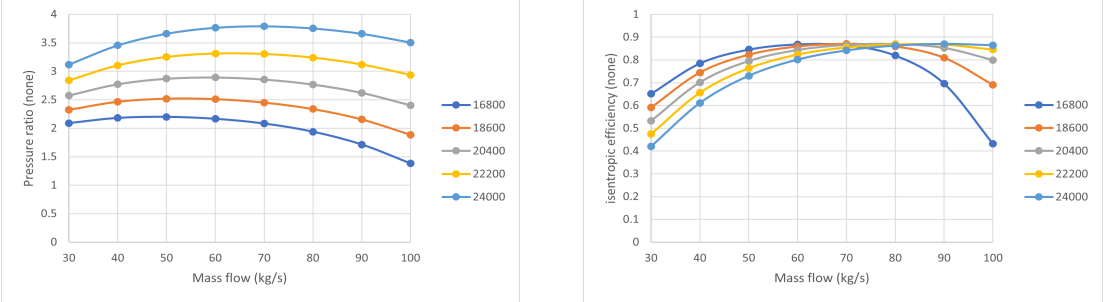

(a) 10 MW_e compressor pressure ratio map (b) 10 MW_e compressor isen. efficiency map

Figure 3-13: Pressure ratio and isentropic efficiency maps with 5 speed lines using Dyreby's methodology [13]. The nominal compressor shaft speed at the design point is 24,000 rpm.

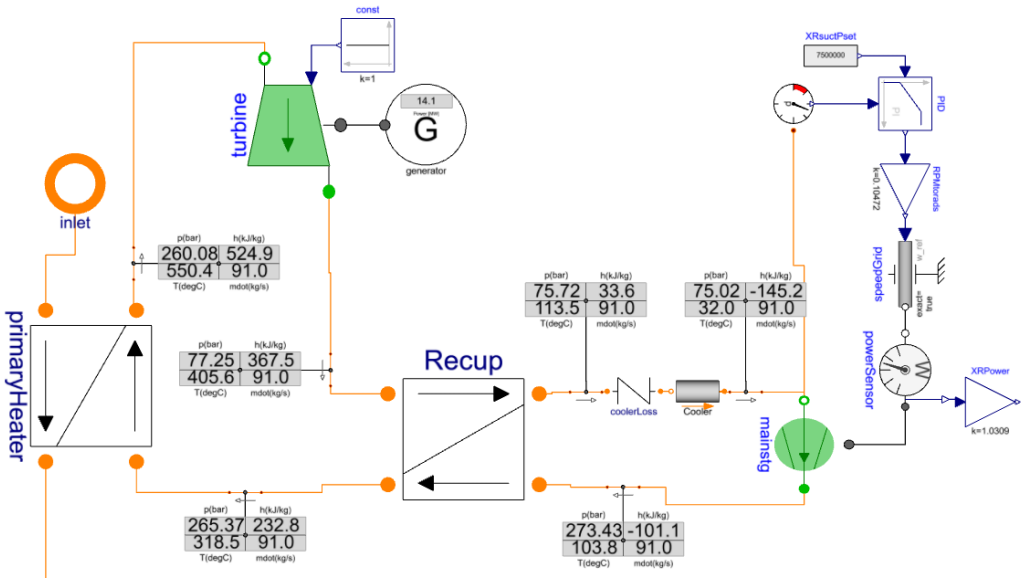

Figure 3-14: The full 10 MW_e sCO_2 cycle. Values shown are at design point.

compressor suction pressure at 75 bar, so that the CO_2 stays in the supercritical regime. Without this PID controller in place, the compressor suction pressure would drop below 75 bar when there is a reduction in the particle mass flow rate to the system resulting in a reduction in heat input to the system, causing a reduction in volumetric flow rate through the cycle. The effect of this control system when the desired power output from the cycle is only 4 MW_e is shown below, with the compressor shaft speed displayed: With the hardware and software models required for simulating design and off-design points in place, the lookup table for the 10 MW_e cycle can be generated. The minimum operating point of this cycle is assumed to

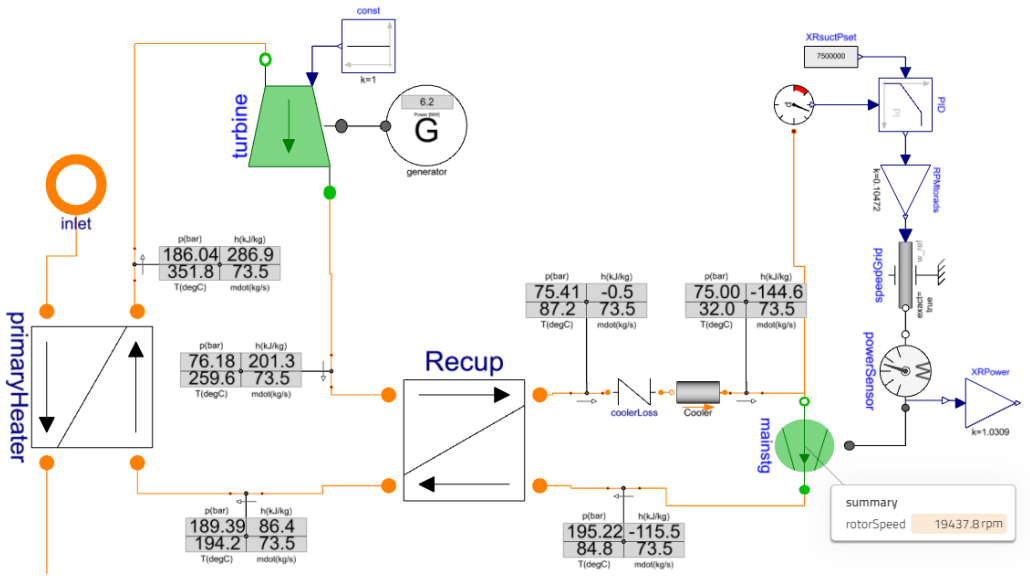

Figure 3-15: 10 MW_e sCO_2 cycle at the 4 MW_e off-design point

40%, i.e. the cycle can not produce less than 4 MW_e net power. This assumption is in place mainly because surge was not accounted for in the compressor model.

The 100 MW_e sCO_2 cycle model

The 100 MW_e sCO_2 cycle, associated with the 100 MW_e "build large" approach, was assumed to be the recuperated recompression variant. The layout of the this variant is shown in figure 2-9b. This cycle was chosen because it is on the Pareto frontier for LCOE for a power block with a net efficiency between 39% and 41% in figure 3-11. Although it is more complicated than the simple recuperated cycle, it is more efficient because the recuperators are split up to ensure better matching between the heat transfer properties of the cold fluid and the hot fluid. Although it has more equipment (one additional compressor and heat exchanger) compared to the simple recuperated variant, it seemed to be better suited to a "build large" theme of higher initial capital for better system performance at scale than the simple recuperated variant. For this cycle, much of the same assumptions used for the 10 MW_e cycle in the previous subsection were used:

- The turbine inlet pressure was assumed to be 260 bar.
- The TIT was assumed to be 550 °C.

- Exchanger pressure and heat transfer performance
  - Both the high temperature recuperator and low temperature recuperator have the same assumptions on pressure drops - 3% on the high pressure side, 2% on the low pressure side. Both are also designed for a 10 °C TTD at the design point, and the resulting areas are 850 m^2 and 500 m^2 for the high temperature and low temperature recuperators respectively. The same Reynolds-based correlation in Modelon Impact was used.
  - For the particle heat exchanger, the 2% pressure drop assumption on the sCO_2 pass remained, along with the 50 °C TTD heat transfer performance which corresponded to a heat transfer area of 8500 m^2. The heat transfer coefficient methodology for the sCO_2 side and the particle side are the same as what was used for the 10 MW_e case.
  - The cooler has the same 0.6% pressure drop on the sCO_2 pass with the same LMTD of 7.2 °C.
- The main compressor's inlet pressure was assumed to be 75 bar.
- The main compressor's inlet temperature was assumed to be 32 °C.

The introduction of the recompressor introduces a new degree of freedom, the recompression flow fraction. Instead of the main compressor doing all of the compression work in the simple recuperated cycle, the recompressor handles some of the flow in the recompression variant. The recompression flow fraction was assumed to be 0.35 at the design point per Heller et al [21].

With the addition of a third turbomachine, the recompressor, to the pre-existing turbine and main compressor, the procedure for designing and parameterizing these components is similar to the process used for the 10 MW_e cycle components with a few differences:

1. The isentropic efficiency of the turbine is still 0.91 and the efficiency of the connected generator is still 0.987. With these values and the cycle pressure

profile, the turbine outlet temperature and the power generated by the turbine+generator at varying mass flow rates through the turbine can be calculated.

2. Now, the isentropic efficiency of the main compressor is still 0.87 at the design point, and the efficiency of the attached motor is 0.97. With the addition of the recompressor, the recompressor isentropic efficiency is assumed to be 5 points lower, or 0.82 at the design point, and the efficiency of the attached motor is 0.97. Using these values, the assumption on recompression flow fraction, and the cycle pressure profile, the power consumed by the main compressor+motor and the recompressor+motor at varying total sCO_2 mass flow rates can be calculated.

3. The mass flow through the turbine and the combined mass flow through the main compressor and recompressor are set equal and the mass flow is manually iterated until the net power (the sum of the power generated by the turbine+generator, the power consumed by the main compressor+motor and the power consumed by the recompressor+motor) matches the design point, in this case 100 MW_e.

4. Both the recompressor and compressor speeds at design point are manually itereated to achieve a specific speed Ns of approximately 60 and a specific diameter Ds of 2.5.

5. The main compressor and recompressor maps are built for 5 speed lines using the same nondimensional methodology referenced in the parameterization of the 10 MW_e compressor. The map design process yields the following in figure 3-16 for the main compressor and figure 3-17 for the recompressor.

With the turbomachinery parameterized, the entire cycle can now be modeled at the design point (100 MW_e) in figure 3-18. The final element of the cycle required to automatically resolve off-design points is the control system. Similar to the 10 MW_e

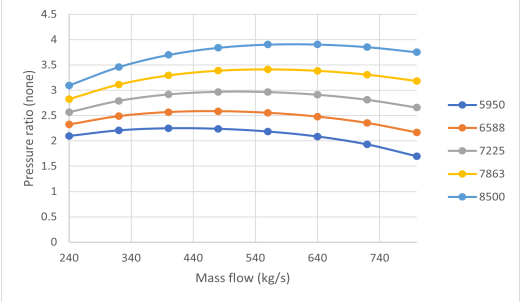

(a) 100 MW_e main compressor pressure ratio map

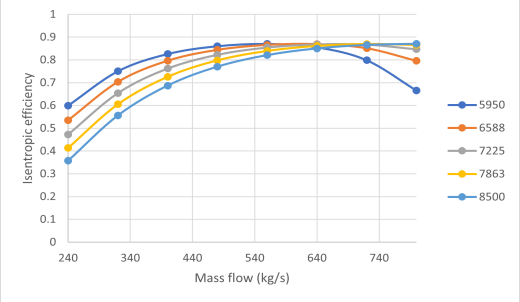

(b) 100 MW_e main compressor isen. efficiency map

Figure 3-16: Main compressor pressure ratio and isentropic efficiency maps with 5 speed lines using Dyreby's methodology [13]. The nominal shaft speed at the design point is 8,500 rpm.

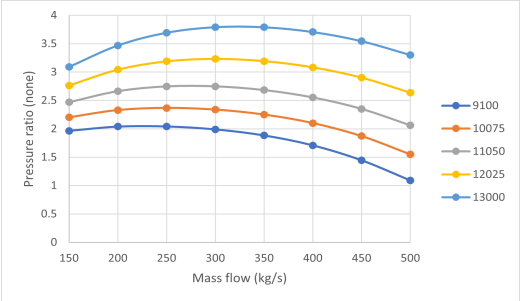

(a) 100 MW_e recompressor pressure ratio map

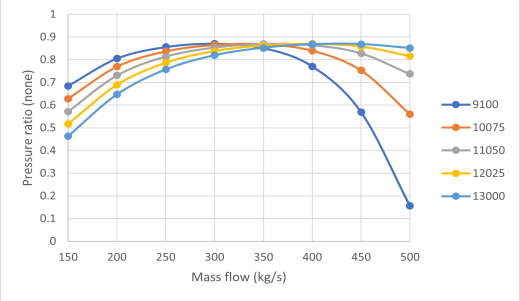

(b) 100 MW_e recompressor isen. efficiency map

Figure 3-17: Recompressor pressure ratio and isentropic efficiency maps with 5 speed lines using Dyreby's methodology [13]. The nominal shaft speed at the design point is 13,000 rpm.

cycle, part of the 100 MW_e cycle control system uses a PID controller to simultaneously reduce the speed of the compressor and proportionally reduce the speed of the recompressor to control the main compressor's suction pressure at 75 bar, to achieve the same goal of keeping the CO_2 in the supercritical regine. The proportion that the recompressor is reduced by is the ratio of the design speed of the recompressor (13,000 rpm) to the design speed of the main compressor (8,500 rpm), or approximately 1.53. The other part of the cycle control system uses a PID controller to increase the recompression flow fraction as the net power generated by the cycle drops, under the assumption that high recompression flow fractions are favored at turndown. A valve at the suction to the recompressor opens to admit more flow as the net power gen-

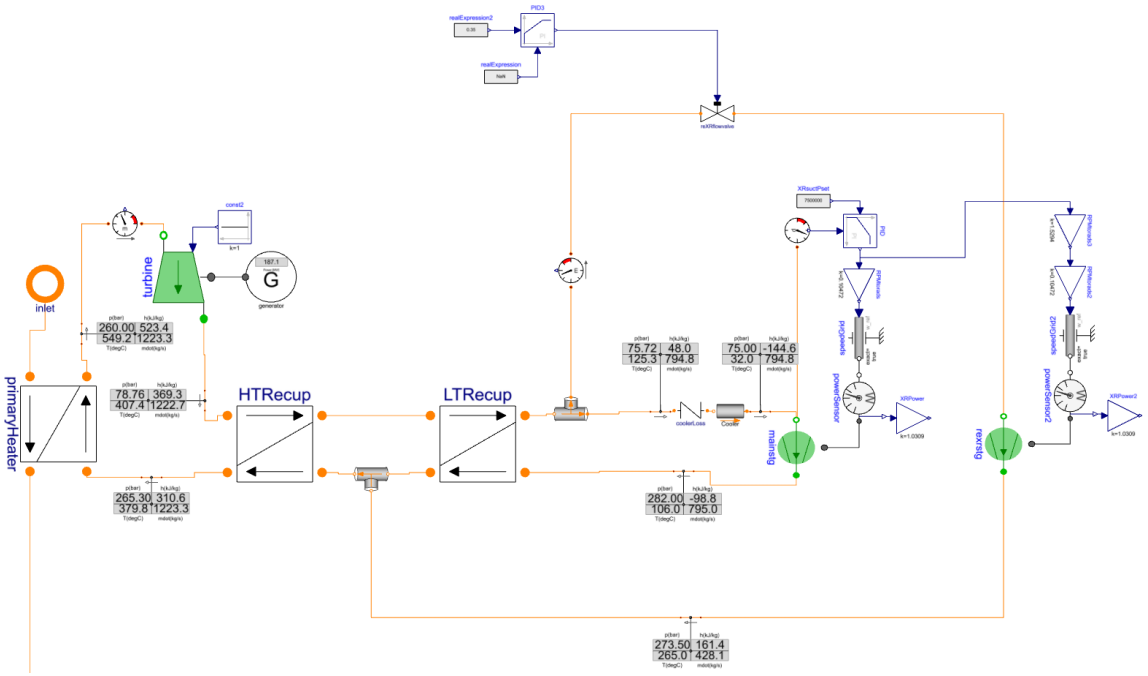

Figure 3-18: The full 100 MW_e sCO_2 cycle. Values shown are at design point.

erated by the cycle reduces. The effect of the 100 M_e cycle control system when the desired power output is 50 MW_e is shown below, with the main compressor and recompressor shaft speed displayed.

The cycle control system uses a PID controller to reduce the speed of the compressor to control the compressor suction pressure at 75 bar, so that the CO_2 stays in the supercritical regime. Without this PID controller in place, the compressor suction pressure would drop below 75 bar when there is a reduction in the particle mass flow rate to the system resulting in a reduction in heat input to the system, causing a reduction in volumetric flow rate through the cycle. The effect of this control system when the desired power output from the cycle is only 4 MW_e is shown below, with the compressor shaft speed displayed. With the hardware and software models required for simulating design and off-design points in place, the lookup table for the 100 MW_e cycle can be generated. The minimum operating point of this cycle was originally assumed to 40% following the assumption used for the 10 MW_e cycle, but the cycle would not converge below a 50% operating point. Therefore, the minimum turndown of this cycle is 50%, so the minimum power level is 50 MW_e.

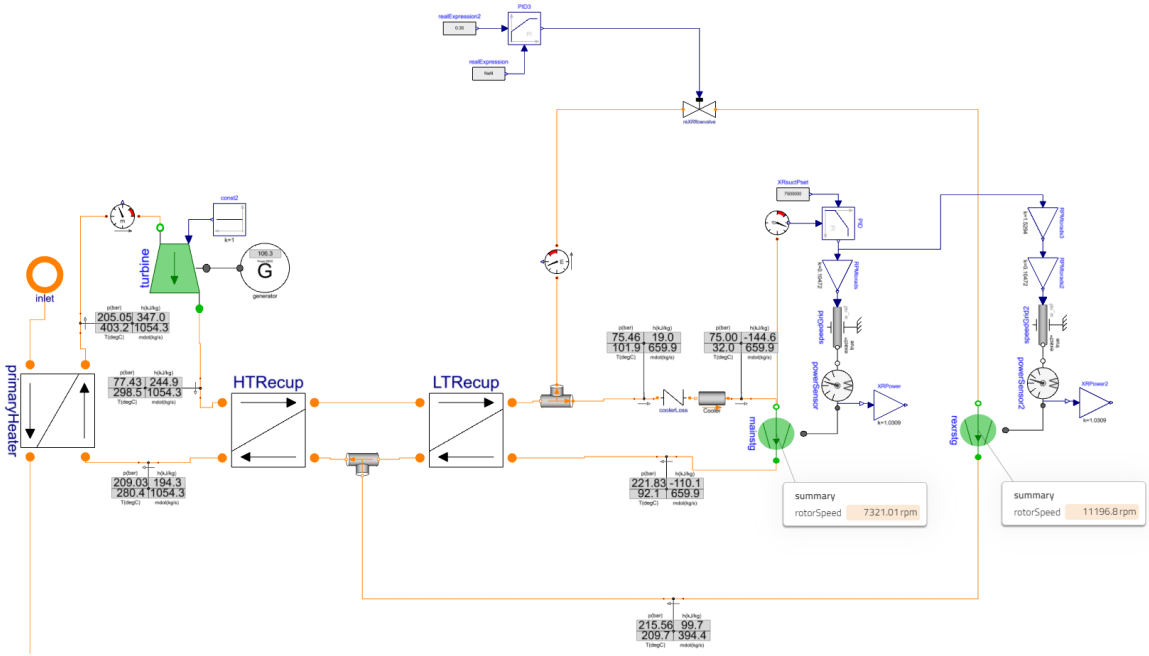

Figure 3-19: 100 MW_e sCO_2 cycle at the 50 MW_e off-design point

3.2.9 Plant Master Control Block

The plant master control block is the software that controls the hardware represented by the different component models. At an abstract level, its job is to control the plant to meet the plant's objectives, including keeping the different components within specified constraints.

For the Gen3 solar tower CSP plants modeled in this work, the main objective is to attempt to generate power around the clock year-round and therefore minimize the amount of time when the plant isn't generating any power. Note that this selected objective is in conflict with other valid objectives - an objective to only generate power at the maximum possible efficiency (i.e. design point operation only) would necessarily incur more time when the plant isn't generating power. The other objectives this system is trying to meet are as follows:

- Keep the particles exiting the receiver at a constant temperature. If the temperature of the particles exiting the receiver were allowed to vary significantly, the performance of the sCO_2 power block could suffer and asset damage to the power block could result (however, this consequence wasn't modeled). Further-

more, the approach for abstracting the sCO_2 cycle into a lookup table would become significantly more complicated.

- Do not overfill the hot silo. In a real plant, if the hot silo were overfilled, hot (nominally 750 °C) particles could escape containment and either cause personnel injury or asset damage.

- Do not allow the cold silo to run empty. In a real plant, if the cold silo ran empty, there wouldn't be enough particles to lift and flow through the receiver to keep the receiver below 750 °C. If that occurred in a real plant, the heliostat field would have to be defocused off the receiver to avoid melting the receiver and other equipment in the proximity.

These objectives are the same for the 10 MW_e and 100 MW_e plants.
The block diagram for the plant control is shown in figure 3-20. The different control loops are as follows:

1. Field power control loop - The field power control loop moderates the power delivered to the receiver from the heliostat field. First, it does a logic check to ensure the power from the field is greater than 1 kW. If the power from the field is not greater than 1 kW then the heliostat field is considered defocused and the power to the receiver is set to zero. Next, the hot silo is checked to see if it is at 90% level or higher. If the hot silo is below 90%, the power to the receiver isn't moderated in any way, but if the hot silo is above 90%, the power to the receiver is forced to zero.

2. Particle receiver exit temperature control loop - the particle exit temperature loop moderates the flow of particles from the cold silo to the hot silo via the particle lift, passing through the receiver on the way. The PI controller that performs this task has a setpoint of 750 °C (or 1023.15 K) and senses the temperature of the particles exiting the receiver. By nature, it is an inverse controller because the sensed variable (the temperature of the particles exiting the receiver) decreases when the output of the controller (the flow of particles

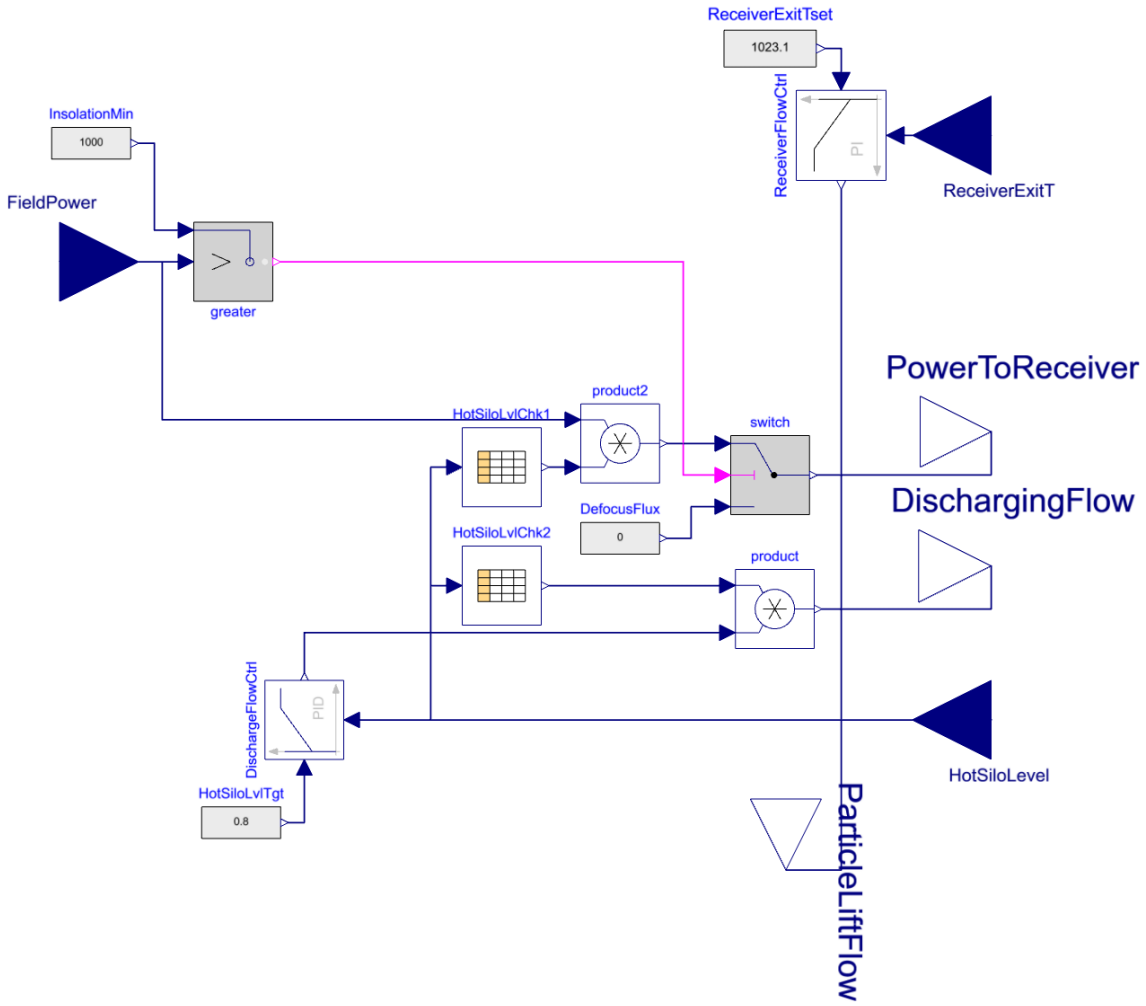

Figure 3-20: Plant master control block for a Gen3 solar tower CSP plant

to the receiver) increases. It is limited to a maximum flow of 3x the particle flow rate at the design point through the sCO_2 power block. For example, if the particle flow rate through the 10 MW_e power block is 64.2 kg/s at the 10 MW_e design point, then the maximum flow allowable through the particle lift is 192.6 kg/s.

3. Particle flow rate through the power block control loop - this loop moderates the flow of particles from the hot silo to the cold silo pssing through the power block. The PI controller that performs this task has a setpoint of 80% and senses the current level in the hot silo. This is also an inverse controller because the sensed variable (the level in the hot silo) decreases when the output of

the controller (the flow of particles to the power block and cold silo) increases. The PI controller is initially constrained between the nominal particle flow rate through the power block at the design point and the particle flow rate through the power block at maximum turndown. For example, for the 10 MW_e sCO_2 power block, the particle flow rate at the nominal 10 MW_e design point is 64.2 kg/s and the flow rate at maximum turndown is 25.1 kg/s, so the output of this first PI controller is constrained between 25.1 kg/s and 64.2 kg/s - no lower or higher. Before the signal is sent to the flow controller between the hot silo and the cold silo, there is a check to ensure the hot silo is at least 10% full. As long as the hot silo is at least 10% full, the signal to the flow controller between the hot silo and the cold silo is unaffected. However, if the hot silo is less than 10% full, the signal to the flow controller is forced to zero.

All of the PI controllers in the aforementioned control loops were tuned manually to minimize overshoot while maintaining an adequate response time to disturbances.

3.3 Validation of the plant model implementation in Modelon Impact

Since there are no Gen3 solar tower CSP plants to directly validate either the 10 MW_e or the 100 MW_e plant model implementations against, validation of the plant model implementations must be done against Gen1 and Gen2 solar tower CSP plants with similar capacity factors.

3.3.1 10 MW_e plant validation

The Planta Solar 10 CSP plant in Spain is a Gen1 solar tower CSP plant (water as the heat transfer fluid with a steam power generation block) with a nominal 11 MW_e power generation capacity, 1 hour of storage, an expected generation rate of 23.4 GWh/year (23,400 MWh/year) and a solar field aperture area of 75,000 m^2 [17].

This resolves to a CF of approx. 24%. It is located in Andalusia, Spain which receives 6.0-6.5 kWh/sq.m/day according to METEOSAT satellite data [32].

The 10 MW_e plant studied in this report is a Gen3 solar tower CSP plant with a nominal 10 MW_e power generation capacity and 16 hours of storage (at minimum turndown). The CF that most closely matches to an expected generation rate of 23,400 MWh/year is between 20% (17,520 MWh/year) and 30% (26,280 MWh/year). Out of the 3 locations of interest (Boston, New Orleans, Daggett), Andalusia is between Daggett (7.5-8.0 kWh/sq.m/day) and New Orleans (5.0-5.5 kWh/sq.m.day). According to this table which was modified from an earlier part of this chapter, a

10 MW_e plant location	20% CF	30% CF
Daggett, CA	55,000 m^2	77,000 m^2
New Orleans, LA	83,000 m^2	117,000 m^2

Table 3.7: Heliostat field area required for 20% and 30% CFs in Daggett, CA and New Orleans, LA

CF between 20% and 30% and in between Daggett and New Orleans would require on the order of magnitude of between 70,000 m^2 and 90,000 m^2 of heliostat area. Considering that the Planta Solar 10 CSP plant has an actual heliostat field area of 75,000 m^2, this is within the 70,000 m^2 and 90,000 m^2 quoted. Therefore, despite having to make a comparison between a Gen1 and a Gen3 solar tower CSP plant it can be assumed that the 10 MW_e plant model implementation in Modelon Impact described in this work is a reasonable approximation for a solar tower CSP plant.

3.3.2 100 MW_e plant validation

The validation of the 100 MW_e plant model implementation in Modelon Impact is somewhat more straightforward because there are more benchmarks for 100 MW_e CSP plants than 10 MW_e plants.

The Crescent Dunes CSP plant in the US is (or was) a Gen2 solar tower CSP plant (molten salt as the heat transfer fluid with a steam power generation block). It has a nominal 110 MW_e power generation capacity, 10 hours of storage, and an expected

generation rate of 500 GWh/year (500,000 GWh/year) for a solar field aperture area of 1,197,148 m^2 [18]. This resolves to a CF of approx. 52%. It is located in Tonopah, Nevada which receives 7.5-8.0 kWh/sq.m/day according to GOES satellite data [32].

The 100 MW_e plant studied in this report is a Gen3 solar tower CSP plant with a nominal 100 MW_e power generation capacity and 16 hours of storage (at minimum turndown). Out of the 3 locations of interest (Boston, New Orleans, Daggett), Daggett is a near exact DNI match for Tonopah, Nevada at 7.5-8.0 kWh/sq.m/day. While this work did not cover a CF of 50%, a one-off simulation was run to estimate the heliostat field area required for the 100 MW_e plant for a 50% CF in Daggett, CA. The required heliostat field area was 1,180,000 m^2, which is an almost exact match to the Crescent Dunes CSP plant's heliostat field area of 1,197,148 m^2. Despite needing to compare a Gen2 and a Gen3 solar tower CSP plant, it can be assumed that the 100 MW_e plant model implementation in Modelon Impact described in this work is a reasonable approximation for a solar tower CSP plant.

3.4 Plant costing

Cost estimates of each plant component are obtained using the correlations in table 2.3. The values of x (W_{th}/K, MW_s, etc.) are reported in the Modelon Impact plant model simulation results. The resulting values are rounded to 3 significant figures in recognition of the level of uncertainty around costs for a low TRL technology like the Gen3 solar tower CSP variant.

3.5 Plant costing validation

NPV is the method by which financial performance of CSP plants is evaluated in this work, but industry data on CSP is provided in terms of LCOE, rather than NPV. Furthermore, the data on the LCOE of CSP is primarily derived from "large approach" i.e. utility scale 100+ MW_e plants.

Therefore, to validate the plant cost correlations, the LCOE will be calculated for

a specific variant (100 MW_e, with a 30% CF, in Daggett, CA) and the results will be compared to industry data to see if the LCOE falls within the expected range that other utility-scale CSP plants are in.

The approximate cost of a 100 MW_e plant with a 30% CF in Daggett, CA is $322 million using the plant costing methodology described previously. The formula for LCOE in [21] is

$$LCOE = \frac{FCR * cost + O\&M_a}{E_{e,a}}$$

Where FCR is 9.37% for a project lifetime of 25 years and an annual interest rate of 8%, the cost is the initial plant cost, $O\&M_a$ is the annual operations and maintenance costs which are assumed to be 2% of the initial plant cost, and $E_{e,a}$ is the annual power produced in kWh, which is 262,800,000 kWh (for a 100 MW_e plant with a 30% CF). Using this methodology, the LCOE is $0.14/kWh, which is well within a reasonable range for recent LCOE of CSP systems at the utility scale ($0.11/kWh -$0.21/kWh), as per IRENA in figure 3-21. Therefore, it can be assumed that the cost correlations and methodology described in this work is a reasonable approximation of the costs of a solar tower CSP plant.

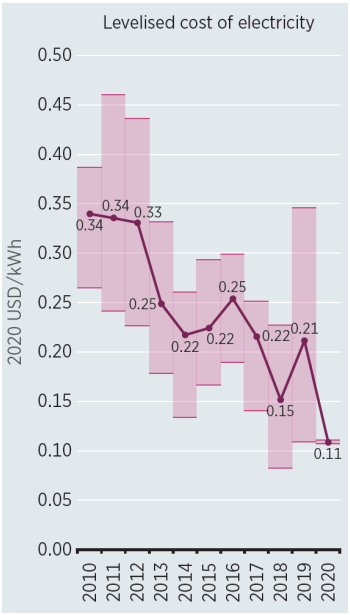

Figure 3-21: LCOE of CSP plants between 2010 and 2020. In the last few years, the LCOE of CSP plants has been between $0.11/kWh to $0.21/kWh. [1]

3.6 NPV calculation with deterministic inputs

To compare the "build large" approach with the "build modular" approach for Gen3 solar tower CSP plants, this work uses NPV as the primary metric and follows the methodology proposed by de Neufville and Scholtes [9]. Although much of the literature uses LCOE to assess the financial performance of CSP and other renewable energy technologies, the LCOE approach involves the use of annuities that do not always include the time-value of money (expressed as the discount rate). The ability to model the time-value of money is critical for evaluating the performance of a "build modular" approach where capital is spent over time rather than all at once. The first part of the analysis compares the NPV of the two approaches using only deterministic inputs across three locations (Daggett CA, New Orleans LA, and Boston MA) and three CFs (20%, 30%, 40%), for a total of nine cases. The fixed inputs to the evaluation, which apply to all nine cases, are as follows:

- Time horizon - assumed to be 25 years, in line with Heller er al [21]. In years 1 to 10, the electricity demand, electricity prices, and number of modules are allowed to vary. From years 11 to 25, these parameters are frozen at the year 10 values to calculate the terminal NPV.

- Yearly operating costs - assumed to be 2% of cumulative capital installed, in line with Heller et al [21].

- Discount rate - assumed to be 9% per NREL's SAM software for molten salt (Gen2) CSP plants [33].

- Learning rate - only applicable to the modular approach, this was assumed to be 10% per the low end of the 10-12% range quoted by [5]. The cost of the nth module is a function of the learning rate and the cumulative production, in accordance with Wright's curve. An example is shown in figure 3-22 below.

- Building time for a module - assumed to be one year. Although this hasn't been demonstrated yet, the SUPCON Delingha 10 MW Tower CSP Project was

Learning rate for modules	
# of 10 MW modules	Cost of the nth module
1	$52.7
2	$47.4
3	$44.6
4	$42.7
5	$41.3
6	$40.1
7	$39.2
8	$38.4
9	$37.7
10	$37.1

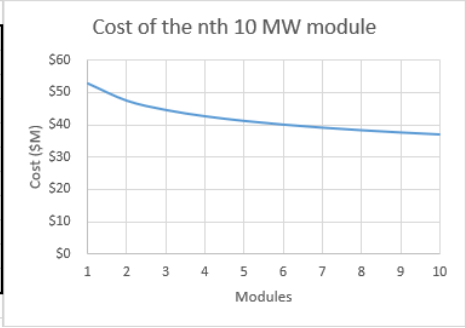

Figure 3-22: The cost of the nth 10 MW_e module if the learning rate is 10% and the first module costs $52.7 million.

started in 2010 and entered operations in 2013 (3 years from start of building to operations), then the Shouhang Dunhuang Phase I - 10 MW Tower CSP Project was started in 2014 and entered operation in 2016 (2 years from start of building to operations) [17], so assuming a one year build time for a module starting in 2022+ may be realistic.

- For the large approach, the large plant is always built and paid for by year 0 so that its full capacity is available in year 1.

The variable inputs to the evaluation that are dependent on the selection of the case (either CF, location, or both) are as follows:

- Demand for electricity - assumed to be the annual electricity production (in MWh/year) of the 100 MW_e plant in year 10. The demand in year 1 is arbitrarily assumed to be 40% of the year 10's demand, and the demand is assumed to be a function of time and increases linearly from year 1 to year 10. From years 11 to 25, the demand is static at the year 10 value to calculate the terminal NPV. The underlying assumption is that the demand for electricity increases over time as the population in the area grows. Since the demand for electricity is related to the annual electricity production of the 100 MW_e plant and the annual electricity production is related to the CF assumed, the profile for electricity demand varies with the CF of the case but not the location.

- Total electricity price - the total price for electricity is the sum of two parts - the base electricity price and a renewable electricity surcharge. The presence of

CF	Year 1 demand	Year 10 demand
20%	70,080 MWh/year	175,200 MWh/year
30%	105,120 MWh/year	262,800 MWh/year
40%	140,160 MWh/year	350,400 MWh/year

Table 3.8: Year 1 and Year 10 demands for different CFs

the renewable electricity surcharge is to represent the fact that some are willing to pay more for electricity generated from a renewable source.

- Base electricity price - the base electricity price at year 1 is assumed to be the most recent residential electricity price in $/MWh. As such, it varies with the location of the case, but not the CF, and is a function of time. The base electricity price through year 10 is assumed to be the linear extrapolation of the best fit linear regression to the data, as shown in figure 3-23 below. From years 11 to 25, the base electricity price is static at the year 10 value to calculate the terminal NPV.

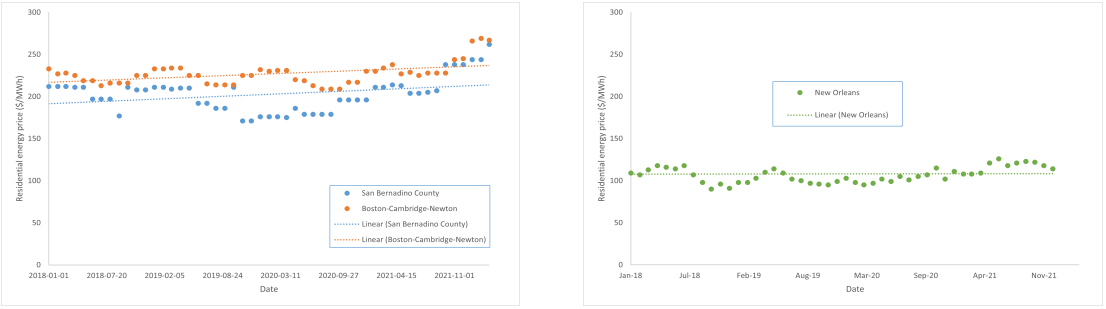

(a) Residential electricity prices in Daggett, CA and Boston, MA with linear regressions. Data from FRED [44] [43].

(b) Residential electricity prices in New Orleans, LA with linear regression. Data from FindEnergy.com [50].

Figure 3-23: Electricity price trends in Daggett, Boston, and New Orleans. The New Orleans data is on a separate graph because the timeframe of the available data is different, because this data came from a different source. The linear regressions are used for extrapolation to year 10 demands.

- Renewable energy surcharge - the renewable energy surcharge is assumed to a linear function of demand. The underlying assumption is that initially at year 1, a fraction of people are willing to pay a surcharge for renewable electricity,

but as the demand increases, the majority will not want to pay a surcharge and the renewable surcharge is zero at the full year 10 demand. From years 11 to 25, the surcharge is zero, as such it is not a factor in the terminal NPV. As demand increases, the renewable energy surcharge falls. The behavior of the renewable energy surcharge varies with both the location and the CF of the case. The value of the renewable energy surcharge at year 1 is estimated using a study showing that some Americans are willing to pay up to \$33.72/month more for renewable energy [19], and data on the electricity consumption in US homes by region (south, west, northeast, midwest) [15]. An example of the renewable energy surcharge and demand versus time follows in figure 3-24.

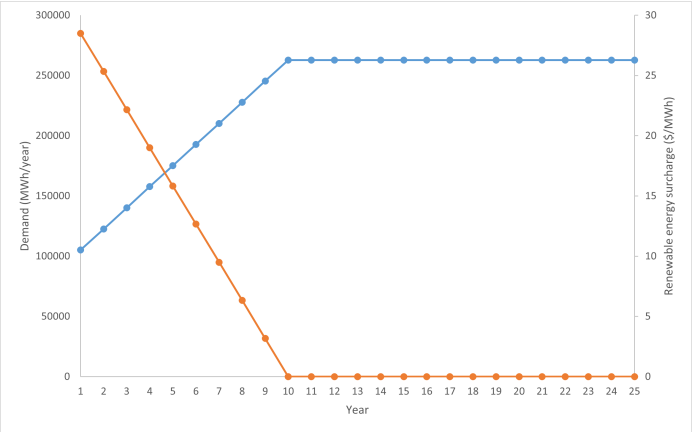

Figure 3-24: Renewable energy surcharge and demand versus time for the Daggett, CA and 30% CF case. The demand is on the left axis, and the renewable energy surcharge is on the right axis. The renewable energy surcharge is inversely related to the demand, by design.

The user-controlled inputs to the evaluation are as follows:

- Decision rule - the decision rule is applied only to the modular approach and dictates under what conditions modules are built. For this work, the decision rule assumes that construction on a new module starts if the existing modules in the current and the past year were at full capacity (i.e. demand is greater than existing capacity). Additional modules are only built one at a time. Since it takes one year for a module to be built, a new module is paid for in the current year but does not actually start generating power until the next year.

- Starting number of modules - the starting number of modules is also only applicable to the modular approach. The starting number of modules (that are built and paid for by year 0, such that their full capacity is available by year 1) in this deterministic evaluation is realistically between 0 and 10 as values above 10 do not make sense since they would exceed year 10 demand. The actual number of starting modules is manually iterated to determine the value that results in the highest NPV. The results of this iteration is shown in the results section for both the deterministic and stochastic NPV calculations.

3.7 NPV calculation with stochastic inputs

While the NPV calculation using deterministic inputs delivers some useful insights into the performance of the "build modular" and the "build large" approach for Gen3 solar tower CSP plants, it does not account for uncertainty. Uncertainty is especially relevant for this low TRL technology with no commercial implementations to date, especially of the modular approach. Therefore, claiming that all of the inputs into the NPV calculation are known and deterministic does not reflect reality as well as incorporating randomness to represent uncertainty in some of the inputs. The following deterministic inputs to the NPV calculation were replaced with probabilistic inputs using the methodology proposed by de Neufville and Scholtes [9]:

- Volatility of the base electricity price - although the linear regressions for the electricity price data over time showed a general slight increasing trend for Daggett and Boston (and a flat line for New Orleans), by visual inspection alone it is clear to see that the linear regressions did not match the data exactly. Year-to-year between years 1 and 10, there are increases and falls in prices, even if the general trend is an increase over time. For years 11 to 25, the price is fixed at the year 10 value. This volatility was simulated by taking the deterministic electricity price data and allowing each point to vary between +25% and -25% randomly. One such example is shown below in figure 3-25.

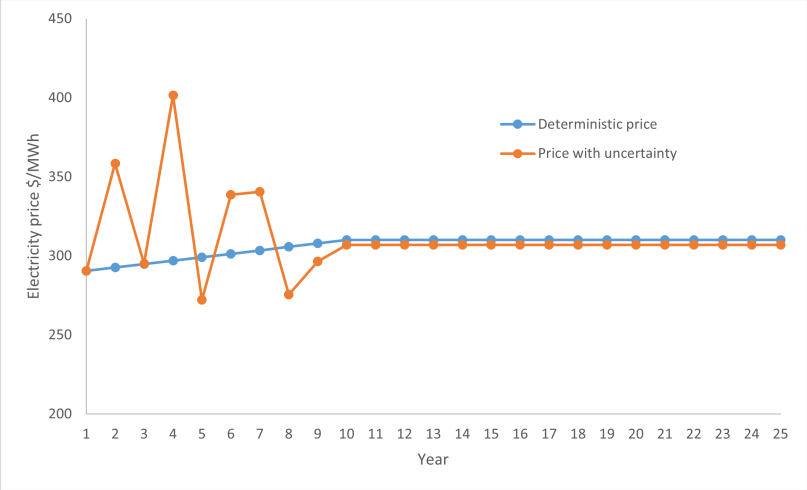

Figure 3-25: Volatility in electricity price. The blue trend is the deterministic price trend, with a trend upwards over time. The orange trend represents one possible outcome of simulating each point on the blue trend varying between +25% and -25% from its "base value" on the deterministic price trend

- Uncertainty in the cost of the first plant - this affects both the "build large" 100 MW_e approach, for which only one plant is built, and the "build modular" x10 MW_e approach, for which multiple 10 MW_e are built. This uncertainty reflects the fact that the actual cost of building the first plant rarely ever matches the estimated cost of the first plant. Normally, the cost of the first plant is higher than the estimated cost, but sometimes it can be lower too. This uncertainty was simulated by allowing the cost of the first plant to vary between -15% and +45% randomly. Although Weiland et al indicate an approximate -30% to +30% [45] in the cost of most equipment, the total 60% range was shifted upwards by 15%, to -15% and 45%. It is assumed that it is more often that equipment costs more than expected rather than less than expected.

- Uncertainty in the learning rate - the learning rate is only applied for the "build modular" approach. This uncertainty is simulated by allowing the learning rate to vary randomly between 10% and 30%, based on the discussion in Chapter 2 on the learning rate.

- Uncertainty in the rate of demand increase - the demand for electricity could increase at a faster rate than projected, perhaps owing to a rapid growth in

population in the area or other factors. This uncertainty was modeled using a triangular distribution, with the deterministic slope of the demand as both the mode and minimum value, and the maximum value as double the deterministic slope of the demand. In doing so, it is assumed that demand is never going to decrease.

- Uncertainty in the relationship (slope) between the renewable surcharge and the demand - the renewable surcharge, which is a function of the demand, could fall at a rate faster than the deterministic slope or be invariant with respect to the demand. The slope of the renewable surcharge with respect to demand is allowed to vary between double the deterministic slope (meaning it falls faster than the deterministic slope) or zero (meaning it is invariant with respect to the demand.

- Variation in the solar energy resource - the weather from year to year is not constant and will not always match the TMY. The variation varies with the region. For the three selected locations, the following data was used with values approximated from figure 3-26:

  - Daggett, CA - 5% volatility
  - New Orleans, LA - 3% volatility
  - Boston, MA - 1.5% volatility

With the uncertainties incorporated into the calculation, a Monte Carlo simulation with 2,000 samples is performed. The results are grouped into 50 bins to produce a cumulative distribution, referred to as a target curve. In the target curve, the probability of different NPVs is shown. Target curves can be overlaid onto each other for comparison. In this work, the target curves for the "build large" and "build modular" approaches are compared. For the "build modular" approach, the number of starting modules is again varied manually to determine the number of starting modules that produces the best P50 NPV (or ENPV) result for the purposes of comparison to the "build large" approach. For the final comparison, a number of

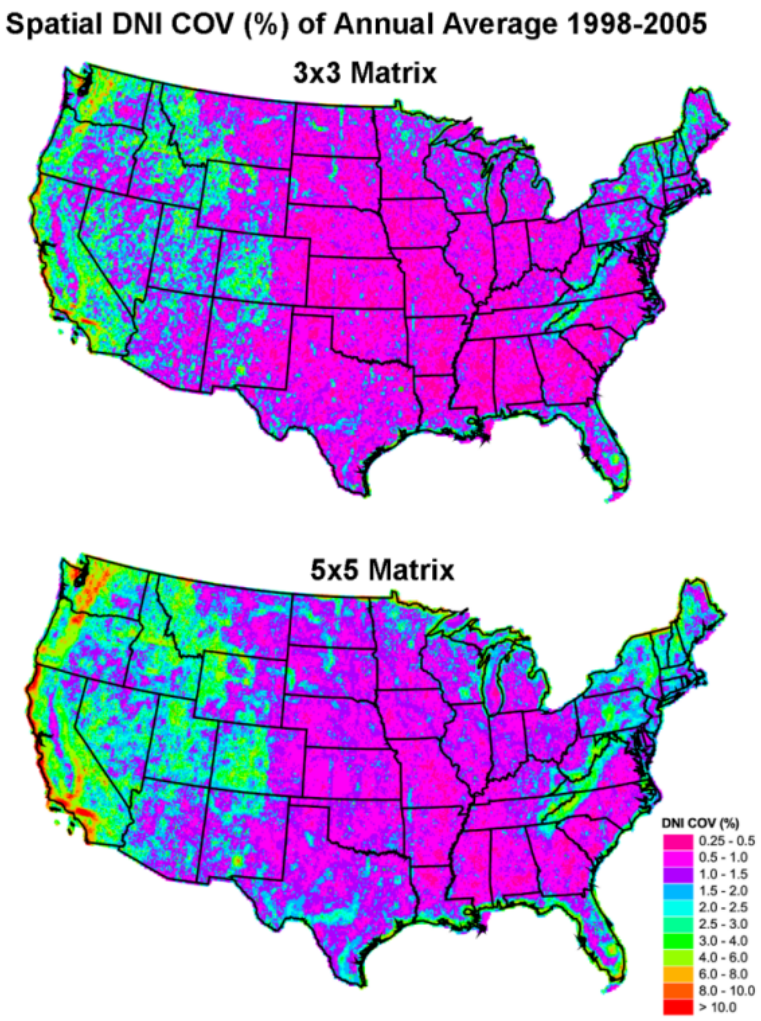

Figure 3-26: DNI annual spatial COV for a 3x3 cell matrix (upper) and a 5x5 cell matrix (lower). From [48]

different dimensions are displayed in addition to the P50 to enable a comparison of the two approaches using multiple dimensions.

Chapter 4

Results

4.1 Plant model implementation results

4.1.1 Simulation speed and computational resource demand

After completing validation, the plant models in Modelon Impact should generate an accurate performance of a Gen3 solar tower plant for an entire year. On a typical desktop computer, the typical runtime and computational resource demand for a single case (a selected location and a selected CF) is as follows:

- Simulated time - 8,760 hours
- Run time - 70-80 seconds
- Function evaluations - 722,156

This equates to 116.8 hours, or 420,480 simulated seconds per real second.

4.1.2 Annual power generated profile

Using the TMY DNI profiles described in 3-4, the model can generate a profile of the annual electrical energy generation, as shown below in figure 4-1. Since the same CF (30%) was used for all three cases, each plant produces the same amount of power in the same time frame. However, the heliostat area required for the plants to deliver

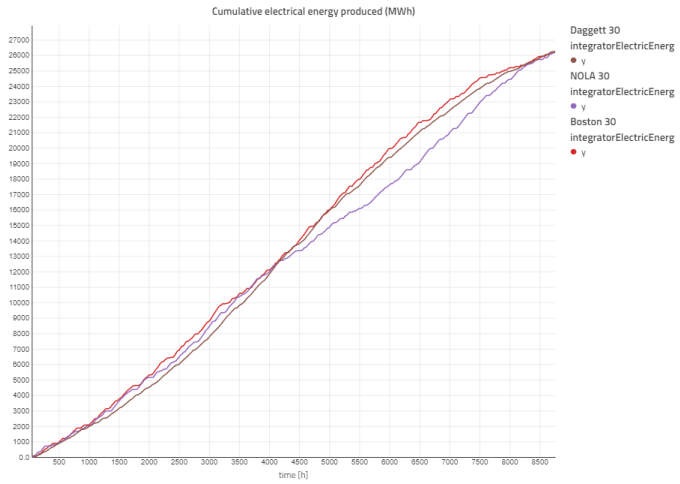

Figure 4-1: Cumulative electrical energy produced (MWh) over the course of a year for 10 MW_e Gen3 solar tower CSP plants in Daggett, Boston, and New Orleans. The CFs are all the same at 30%.

the specified CF in the different locations is very different, with the Boston plant requiring 1.6x the area of the Daggett plant, as referenced in tables 3.3 and 3.4.

The location of the plant has a significant impact on the heliostat area required for the plant. As a result, the performance characteristics of the same 10 MW_e plant in different locations can be very different. For the three locations, a profile of electrical power generated over the year for each of the three locations with the same 30% CF case can be seen in figures 4-2, 4-3, and 4-4. Daggett, CA has a high solar resource

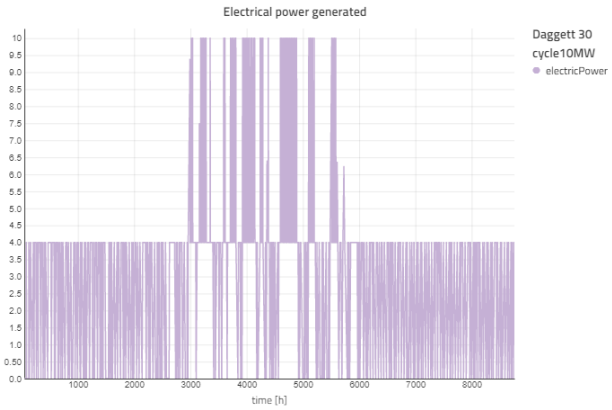

Figure 4-2: Profile of electrical power generated by a 10 MW_e plant in Daggett, CA

so the heliostat area required for this location's 10 MW_e plant to achieve a 30% CF is low. With a low heliostat area, the plant actually operates at nominal power output (10 MW_e) for only a small fraction of the year, mainly in the summer. The rest of

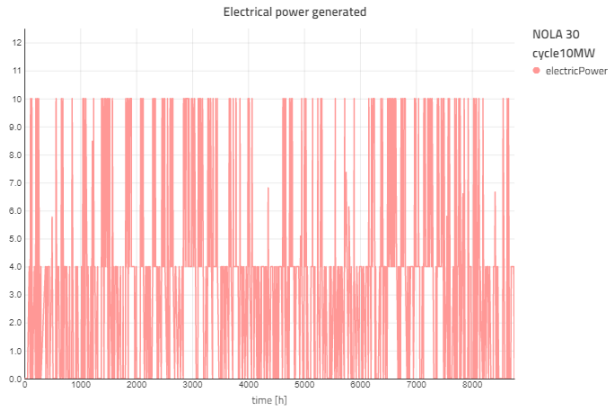

Figure 4-3: Profile of electrical power generated by a 10 MW_e plant in New Orleans, LA

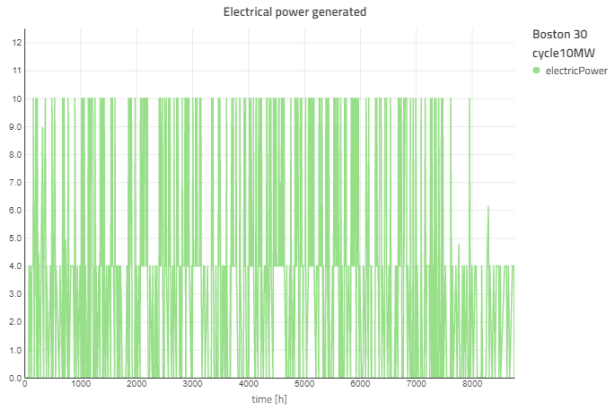

Figure 4-4: Profile of electrical power generated by a 10 MW_e plant in Boston, MA

the time, it is primarily operating in turndown (4 MW_e).

However, for New Orleans and Boston, which have poorer solar resources, the heliostat areas required for the 10 MW_e plants at these locations to achieve a 30% CF is high. Put simply, plants in these locations need a large heliostat area to generate power while the sun is shining, because the sun doesn't shine as often in these areas as in Daggett, CA. Therefore, these plants operate at nominal power output for a larger percentage of the time compared to the same plant in Daggett, CA.

The simulation does not just output electrical power results. Rather, all calculated variables within the model can be saved and trended for the entire length of the simulation. The model results are limited in resolution only by the resolution of the data provided. Since the data was provided in terms of a TMY file with hourly data for an entire year, the model relies on the Akima spline interpolation technique to

report sub-hourly results, as seen in figure 4-5.

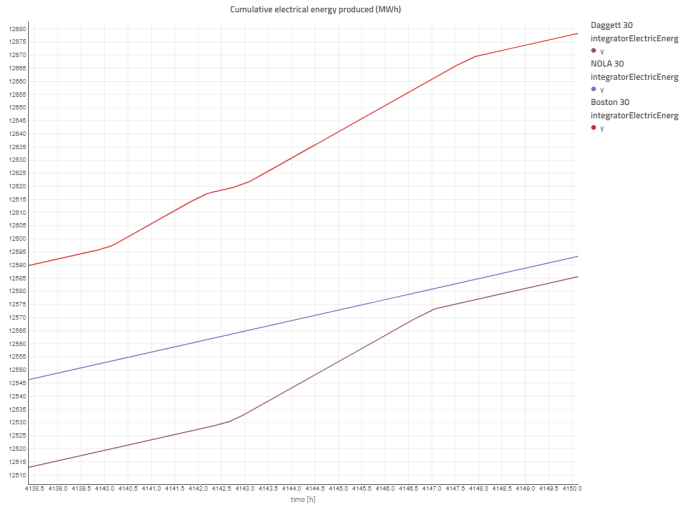

Figure 4-5: Cumulative electrical energy produced (MWh) over the course of 1.5 hours for 10 MW_e Gen3 solar tower CSP plants in Daggett, Boston, and New Orleans. The CFs are all the same at 30%.

4.2 Plant cost model implementation results

The estimated first unit costs (in millions of $) of the 10 MW_e and 100 MW_e plants across all three CFs and three locations are summarized in the following table 4.1, with all costs rounded to three significant figures. The cost breakdowns can be visualized

CF	Location	10 MW_e plant cost ($M)	100 MW_e plant ($M)
20%	Daggett, CA	47.1	291
	New Orleans, LA	51.6	332
	Boston, MA	52.7	344
30%	Daggett, CA	50.6	322
	New Orleans, LA	57	379
	Boston, MA	59.9	401
40%	Daggett, CA	54.3	353
	New Orleans, LA	68	451
	Boston, MA	75.9	502

Table 4.1: Plant costs in different locations and different CFs

in the following figures 4-7 and 4-8. Both figures use a common legend 4-6.

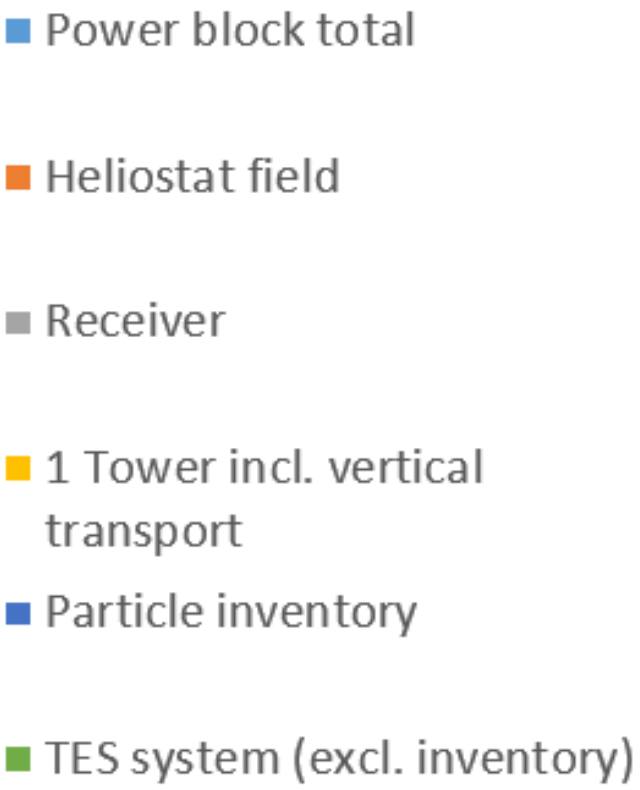

Figure 4-6: Color legend for the doughnut cost breakdown graphs

In the two figures 4-7 and 4-8, the following patterns can be observed:

- Going across the rows (increasing CF), the fraction of plant costs attributed to the heliostat field increases. This is because the heliostat field needs to get larger for the plant to operate at increasing CFs.
- Going across the columns (from Daggett, to New Orleans, to Boston), the fraction of plant costs attributed to the heliostat field increases. This is because the heliostat field needs to get larger as the quality of the solar resource (or available solar energy) decreases.
- In the bottom right case for both figures, the cost of the heliostat field is well in excess of all of the rest of plant costs. This can also be observed as one moves towards the bottom right in both figures.
- Comparing both sets of figures, it appears that the total power block cost makes

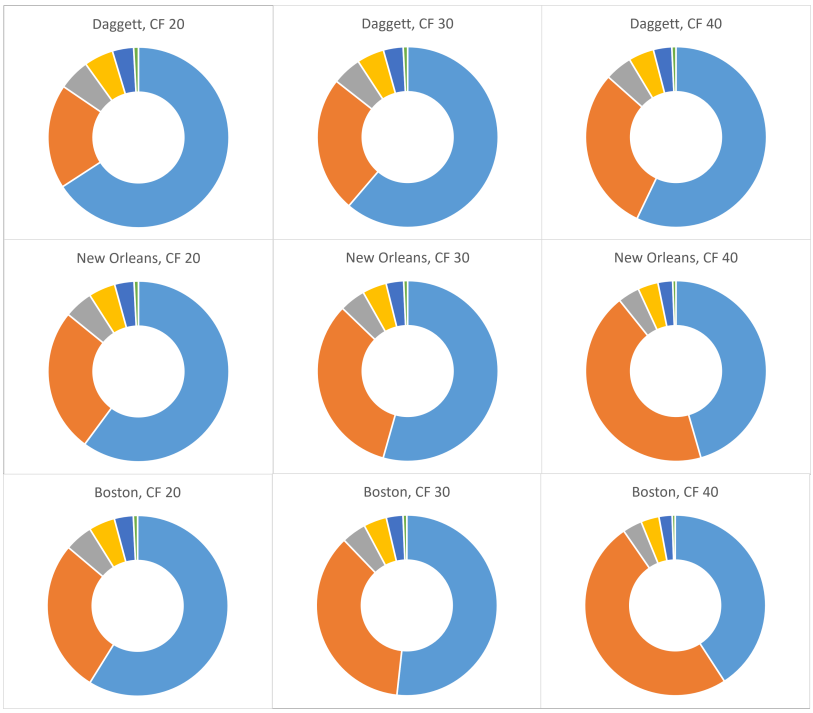

Figure 4-7: Cost breakdowns for all of the 10 MW_e plants in all three locations and three CFs

up less of the total cost for the 100 MW_e plants as it does for the 10 MW_e plants. This is because the cost correlations for the power block equipment incorporate economies of scale, so the cost of the power block equipment doesn't scale as quickly as the cost of the heliostat field and the other plant equipment.

4.3 Results of the NPV calculation with deterministic inputs

Before a table comparing the NPVs of the "build large" (a single 100 MW_e plant) and "build modular" (multiple 10 MW_e plants) approach can be generated, the starting number of modules for the "build modular" approach needs to be specified for each case. The results of sweeping across 11 possible starting number of modules (from 0 to 10 inclusive) over all three CFs and three locations can be found in in the heat map in figure 4-9 below. The data can also be visualized as a set of 9 bar graphs in figure 4-10. Figures 4-9 and 4-10 show that for the Daggett and Boston cases, starting

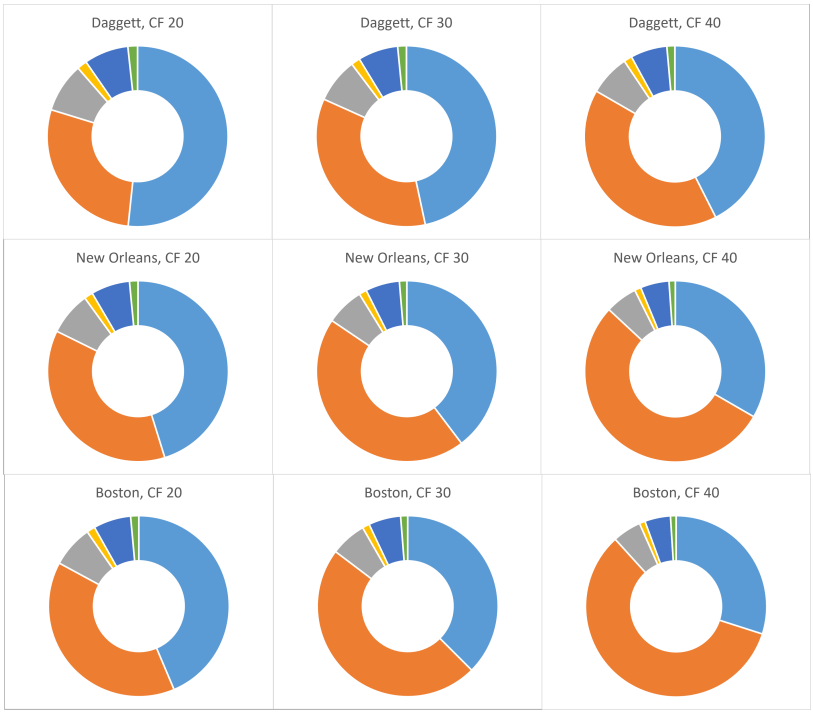

Figure 4-8: Cost breakdowns for all of the 100 MW_e plants in all three locations and three CFs

with 4 modules yields the highest NPV for the modular approach. This is expected for the deterministic case because the demand in year 1 is equal to the capacity of 4 modules. It is also expected that the NPV declines for a starting number of modules less than 4 or greater than 4. When the starting number of modules is less than 4, the demand is higher than the capacity for the first few years and the installed plants are not able to capture the maximum demand (and therefore revenue) for the first few years. When the starting number of modules is greater than 4, the installed generation capacity exceeds the demand for the first few years. As a result, the costs of both building and maintaining the excess and unutilized generation capacity when it isn't needed yet negatively impact the net present value.

For the New Orleans cases, starting with 1 module yields the highest NPV for the modular approach, but it should also be noted that all of the values are very negative. For these cases, although the demand in year 1 starts equal to the capacity of 4 modules just like the Daggett and Boston cases, it is just not worth it to meet year 1's demand with 4 modules. This is because of two reasons:

		Starting number of modules for the "build modular" approach										
	CF (%)	0	1	2	3	4	5	6	7	8	9	10
Daggett	20	-44.8	18.7	27.7	30.0	35.3	28.2	20.4	9.9	-5.1	-26.9	-44.9
	30	57.7	148	180	185	206	190	184	181	166	135	124
	40	159	276	331	339	375	351	346	350	336	294	292
New Orleans	20	-228	-194	-221	-222	-240	-234	-246	-271	-290	-300	-336
	30	-214	-169	-190	-190	-205	-201	-213	-238	-258.4	-272	-308
	40	-236	-178	-199	-197	-212	-209	-223	-251	-275	-293	-334
Boston	20	-66.8	0.3	6.4	8.0	11.2	4.5	4.7	-17.6	-34.7	-57.8	-79.5
	30	19.0	115	142	146	163	148	139	132	114	80.3	64.0
	40	50.1	177	216	223	248	227	216	209	186	142	123

Figure 4-9: Heat map of NPV using deterministic inputs for the "build modular" approach with a varying number of starting modules for different CFs and locations.

1. The solar resource in New Orleans is worse than that of Daggett, which means that a 10 MW_e module designed for any CF will cost more in New Orleans than in Daggett. Therefore, the cost of each module in New Orleans is relatively high compared to the same module in Daggett.

2. The typical price of residential electricity in New Orleans ($114/MWh in year 1 [50]) is much lower than the same for Daggett ($262/MWh in year 1 [44]) or Boston ($267/MWh in year 1 [43]). Therefore, the revenue for providing residential electricity in New Orleans is much lower than the revenue in Daggett or Boston.

As a result, the optimum number of starting modules in the "build modular" approach in New Orleans is more about limiting losses than capturing revenue. Therefore the optimum number of starting modules in New Orleans reflects a strategy of building a minimum number of modules early and deferring the rest to future years where the costs are discounted.

After determining the optimum number of starting modules for each case, the deterministic NPV of the "build modular" approach can be compared with the "build large" approach. The NPV for the two approaches across all three CFs and three locations using deterministic inputs are summarized in the following table 4.2, with all NPVs rounded to three significant figures. From these results, it can be observed that under deterministic conditions, the "build large" approach has a higher NPV than

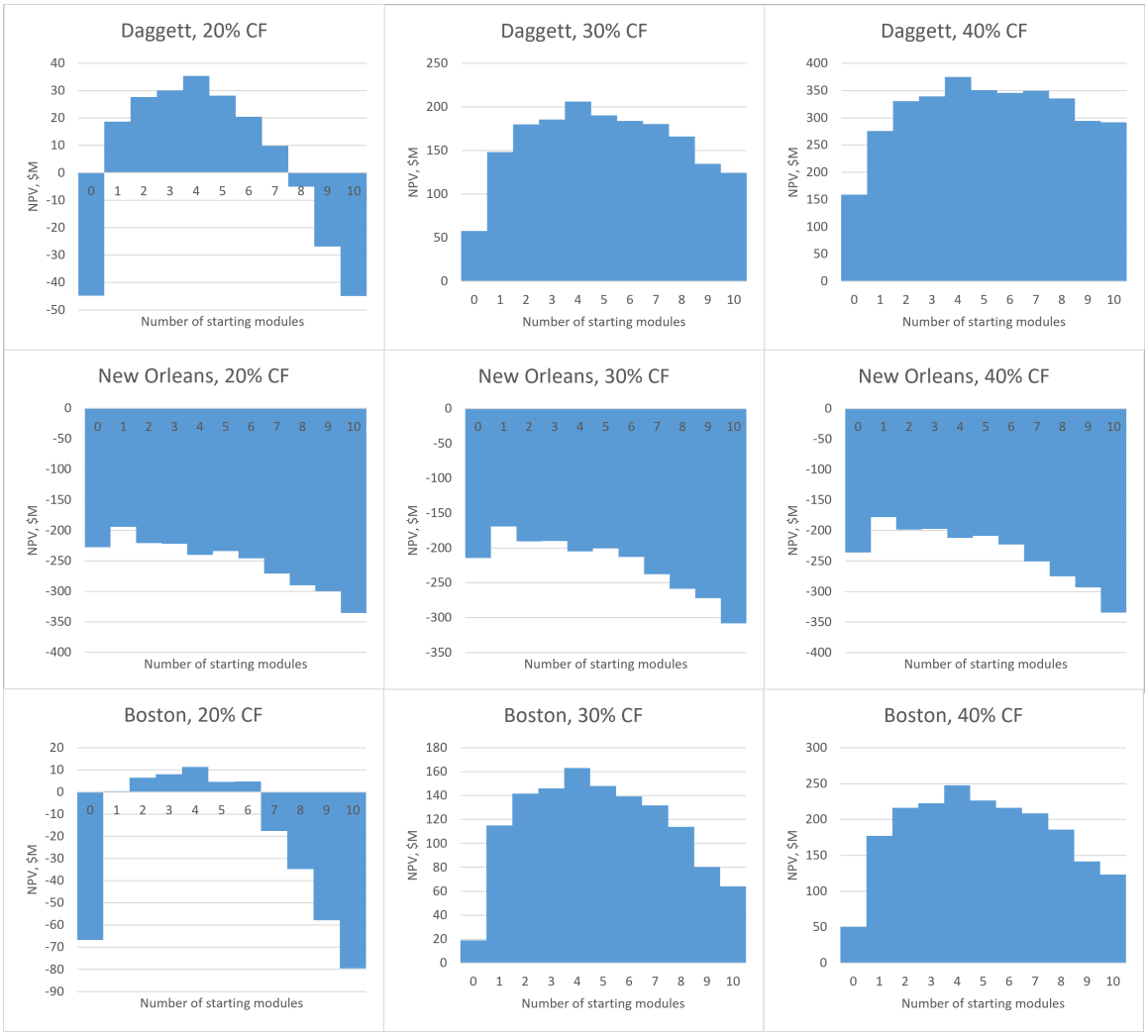

Figure 4-10: Bar graphs for each of the 9 cases showing how the number of starting modules affects the deterministic NPV of the modular approach.

the "build modular" approach in most cases, with the exception of the New Orleans cases and the 30% CF Boston case. This aligns with current CSP industry knowledge that "bigger is better" under deterministic conditions, as large plants benefit from economies of scale in the cost of equipment. So far, CSP plants have only been seriously considered in the southwestern US (e.g. where Daggett is located), so the behavior of the two approaches for the Daggett cases is more relevant than for the New Orleans and Boston cases.

For the New Orleans cases where this is not the case, the NPVs are all firmly in the negative. Although the "build modular" approach outperforms the "build large" approach here, the location is so unfavorable to CSP plants (due to the middling

CF	Location	"Build large" approach NPV ($M)	"Build modular" approach NPV ($M)
20%	Daggett, CA	57.4	35.3
	New Orleans, LA	-239	-194
	Boston, MA	13.0	11.2
30%	Daggett, CA	223	206
	New Orleans, LA	-217	-169
	Boston, MA	157	163
40%	Daggett, CA	389	375
	New Orleans, LA	-224	-178
	Boston, MA	249	248

Table 4.2: NPV comparison of both approaches across CFs and locations

quality of the solar resource and the low residential price for electricity) that it does not seem to be worthwhile for either CSP approach here.

For the Boston cases, where the solar resource is relatively poor but the price of residential electricity is high, the "build modular" approach performs similarly to the "build large" approach, and even exceeding it in the 30% CF case. For the 30% CF case in particular, the performance of the "build modular" approach relative to the "build large" approach here is likely an anomaly attributed to slight advantage in turndown the 10 MW_e sCO_2 cycle has over the 100 MW_e sCO_2 cycle (turndown to 40% versus a turndown to 50%, meaning the 10 MW_e sCO_2 can generate power for more time than the 100 MW_e sCO_2 cycle) and the fact that the required heliostat area for the both plants increases nonlinearly between CFs of 20% and 30% (figures 3-5) due to the poor solar resource.

4.4 Tornado chart based on the NPV calculation with deterministic inputs

Before introducing uncertainty into the NPV calculation, it is important to understand each variable's expected range of uncertainty and how the low and high values of this range affect the NPV calculation. By doing this, the variables that have the largest effect on the NPV can be identified. The following tornado diagram in figure 4-11 captures both the effect of range and rate of change for selected variables on the

NPV. In table form, the inputs used to create this tornado chart follow the chart.

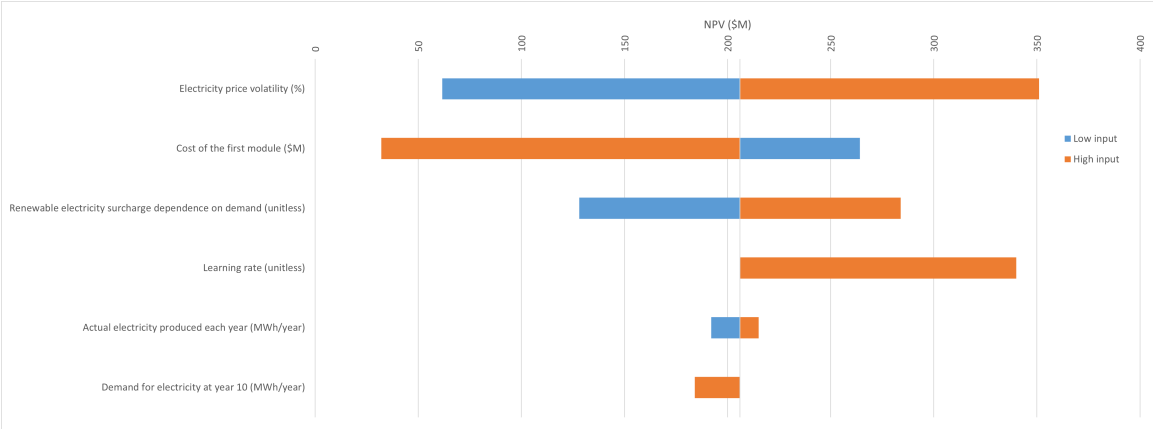

Figure 4-11: Tornado chart for the "build modular" approach for a 30% CF in Daggett.

Variable	Initial input	Low input	High input	Low result ($M)	High result ($M)
Base electricity price volatility (%)	0%	-25%	+25%	61.6	351
Cost of the first module ($M)	50.6	43.0	73.4	264	32.0
Renewable electricity surcharge dependence on demand (none)	-0.00018	-0.00036	0	128	284
Learning rate (none)	0.1	0.1	0.3	206	340
Actual electricity produced per module per year (MWh/year)	26,280	24,966	27,594	192	215
Demand for electricity at year 10 (MWh/year)	262,800	262,800	525,600	206	184

Table 4.3: Data used to build the tornado chart

Although the tornado diagrams for CFs other than 30% and/or other locations other than Daggett and/or the "build large" approach might have different values, the absolute values in the graph aren't as important as their importance relative to each other. (Also, the "build large" approach wouldn't include the learning rate). Therefore, only 1 tornado chart is shown here for the purposes of showing an example.

From the top down, it can be observed that:

- Volatility in the base electricity price has a large effect on the NPV, which is expected. Since the volatility is in both directions the effect on the NPV is centered on the reference NPV value of $206M.

- The next highest effect comes from the cost of the first module, which is lopsided because it is assumed that it is more likely to cost more than estimated rather than less than estimated.

- The renewable electricity surcharge dependence on demand is next as it is another impact on the total electricity price.

- The learning rate, which is specific to the "build modular" approach, is next. Here, the initial input and the low range input are already equal and match the most conservative estimates of CSP learning rates in literature. Therefore, the learning rate can only be equal to or higher than 0.1, and there is only upside here for the higher values.

- The actual electricity produced per module per year reflects the fact that weather is variable and Daggett has a DNI variation of +/- 5%.

- Lastly, the demand for electricity at year 10 seems to have the lowest effect. When the demand is double the initially expected demand in year 10, a higher number of starting modules is favored (in this case, 9) because the simulation is constrained to only allow 1 new module to be built per year. The higher number of starting modules causes high upfront spending that is not discounted, so the effect of this nondiscounted expense balances out the additional revenue from the higher demand and as a result the net effect of a higher demand at year 10 is relatively small and actually negative to the NPV.

4.5 Results of the NPV calculation with stochastic inputs

This section is divided up into multiple subsections.

4.5.1 Specifying the number of starting modules

Similar to the process for the NPV calculation with deterministic inputs, the starting number of modules for the "build modular" approach needs to be specified for each case. As before, the following figures 4-12 and 4-13 shows the result of sweeping across the 11 possible starting number of modules (from 0 to 10 inclusive) over all

three CFs and three locations. However, this time, the values in the table are P50 NPVs or ENPVs. In the heat map and the bar graphs with results derived from

		Starting number of modules for the "build modular" approach										
	CF (%)	0	1	2	3	4	5	6	7	8	9	10
Daggett	20	-49.0	25.0	41.0	57.0	70.0	67.0	64.0	54.0	48.0	37.0	20.0
	30	52.0	153	192	225	255	256	254	244	242	226	216
	40	149	282	343	399	433	449	436	440	433	411	403
New Orleans	20	-231	-190	-202	-219	-232	-234	-239	-252	-265	-278	-291
	30	-220	-158	-172	-181	-186	-192	-197	-206	-231	-234	-253
	40	-240	-164	-177	-184	-192	-193	-200	-212	-231	-245	-266
Boston	20	-72.0	11.0	24.0	36.0	42.0	43.0	41.0	31.0	18.0	6.0	-9.0
	30	11.0	120	157	188	212	220	206	204	186	176.0	159.0
	40	37.0	187	238	285	312	317	308	321	291	263	256

Figure 4-12: Heat map of ENPVs using stochastic inputs for selected variables in the "build modular" approach with a varying number of starting modules for different CFs and locations.

stochastic inputs, there are some similarities and differences with the results in the same heat map and bar graphs with results derived from deterministic inputs. The optimum number of starting modules is still 1 for the New Orleans cases just like it was for the deterministic case. For Daggett and Boston, the ENPVs also approach a maximum between 0 and 10 starting modules, just like in the deterministic case.

However, in the stochastic results, 4 starting modules is not always the optimum with respect to ENPV. For several cases such as Daggett CF 30%, Daggett CF 40%, and others, the optimum number of starting modules is 5, and in some cases the ENPV for 6 or even 7 starting modules is higher than that of 4 starting modules. This is likely due to the effect of learning rates higher than 0.1 making the cost of the nth module much cheaper in multiple Monte Carlo runs, which incentivizes the construction of more modules as they are now cheaper and more revenue from higher demand can be captured.

Despite the fact that 5 starting modules technically delivers the highest ENPV, in a stochastic evaluation there are more metrics to consider than just ENPV alone. For this reason, the base case is assumed to be 4 starting modules for the Daggett and Boston cases for two reasons. First, the ENPVs between the range of 4 to 7 starting modules appears to be relatively tightly clustered, i.e. there is a large difference

Figure 4-13: Bar graphs for each of the 9 cases showing how the number of starting modules affects the stochastic ENPV of the modular approach.

between 0 and 4 or 7 and 10, but between 4 and 7 there is not so much difference. Second, the initial capital spend required for deployment is lower for 4 modules than it is for 5, much less 6 or 7. In the interest of keeping the initial capital spend low while also trying to achieve a relatively high ENPV, the base case is 4 starting modules for Daggett and Boston.

4.5.2 Comparing stochastic ENPVs and deterministic NPVs

Building off a previous table 4.2, now the ENPVs using stochastic inputs can be compared with the NPVs using deterministic inputs in two different tables, one for the "build modular approach" and one for the "build large" approach. The first is the

"build modular" approach table. In general, the "build modular" approach has higher

CF	Location	"Build modular" approach deterministic NPV ($M)	"Build modular" approach stochastic ENPV ($M)	%change
20%	Daggett, CA	35.3	70	98
	New Orleans, LA	-194	-190	-2
	Boston, MA	11.2	42.0	275
30%	Daggett, CA	206	255	24
	New Orleans, LA	-169	-158	-7
	Boston, MA	163	212	30
40%	Daggett, CA	375	433	15
	New Orleans, LA	-178	-164	-8
	Boston, MA	248	312	26

Table 4.4: NPVs vs ENPVs for the "build modular" approach

ENPVs using stochastic inputs than the NPVs using deterministic inputs. This is to be expected because the learning rate was fixed at a low value in the deterministic case, but in the stochastic case the learning rate is allowed to be anywhere between the lower value in the deterministic case (0.1) and three times the lower value in the deterministic case (0.3). The only location where this is not true is for the New Orleans cases, where the values are basically equal between the stochastic and deterministic approaches. In these cases, it appears that even higher learning rates are not capable of reducing module costs enough to offset the poor electricity price in the region.

For the "build large" approach table below, the ENPVs are all lower than the NPVs using deterministic inputs. This is to be expected because the cost of the plant, which in the "build large" approach is fully incurred in year 0, is now typically 115% of the deterministic value (it's allowed to be between 85% and 145% of the deterministic value). Although the cost uncertainty was modelled in the same way for the "build modular" approach, the "build modular" approach had the learning rate to counteract the cost overrun effect. However, the "build large" approach does not have any effect to counter the cost overrun effect and as a result the ENPV is worse than the NPVs using deterministic inputs.

CF	Location	"Build large" approach deterministic NPV ($M)	"Build large" approach stochastic ENPV ($M)	%change
20%	Daggett, CA	57.4	31	-46
	New Orleans, LA	-239	-293	-23
	Boston, MA	13.0	-25	-292
30%	Daggett, CA	223	198	-11
	New Orleans, LA	-217	-271	-25
	Boston, MA	157	120	-24
40%	Daggett, CA	389	368	-5
	New Orleans, LA	-224	-287	-28
	Boston, MA	249	211	-15

Table 4.5: NPVs vs ENPVs for the "build large" approach

4.5.3 Comparing ENPVs for "build large" and "build modular"

The following table 4.6 compares the ENPVs for the "build large" and "build modular" approaches. In every case, the "build modular" approach's ENPV is greater than the same for the "build large" approach. Excluding the Boston CF 20% case where the percentage change is high due to the small denominator, the typical percentage increase in ENPV for the build modular approach relative to the build large approach is around 20%.

CF	Location	"Build large" approach stochastic ENPV ($M)	"Build modular" approach stochastic ENPV ($M)	%change
20%	Daggett, CA	57.4	70	22
	New Orleans, LA	-239	-190	21
	Boston, MA	13.0	42	-223
30%	Daggett, CA	223	255	14
	New Orleans, LA	-217	-158	27
	Boston, MA	157	212	35
40%	Daggett, CA	389	433	11
	New Orleans, LA	-224	-164	27
	Boston, MA	249	312	25

Table 4.6: ENPVs for the "build large" and "build modular" approaches

4.5.4 Results for Daggett, CA

The output of the stochastic simulation is a target curve showing a cumulative distribution of NPVs and their probability in the following figure 4-14. In the figure, the "build modular" approaches clearly dominate the "build large" approach at every CF. As the CF increases, the curves shift to the right, but the "build modular" approach target curve beats the "build large" approach target curve in nearly all of

the selected dimensions. These dimensions are shown in the following figure 4-15. In this figure 4-15, the "build modular" approach is favorable compared to the "build large" approach in all dimensions except for the standard deviation, indicating the "build large" approach is relatively more robust than the "build modular" approach.

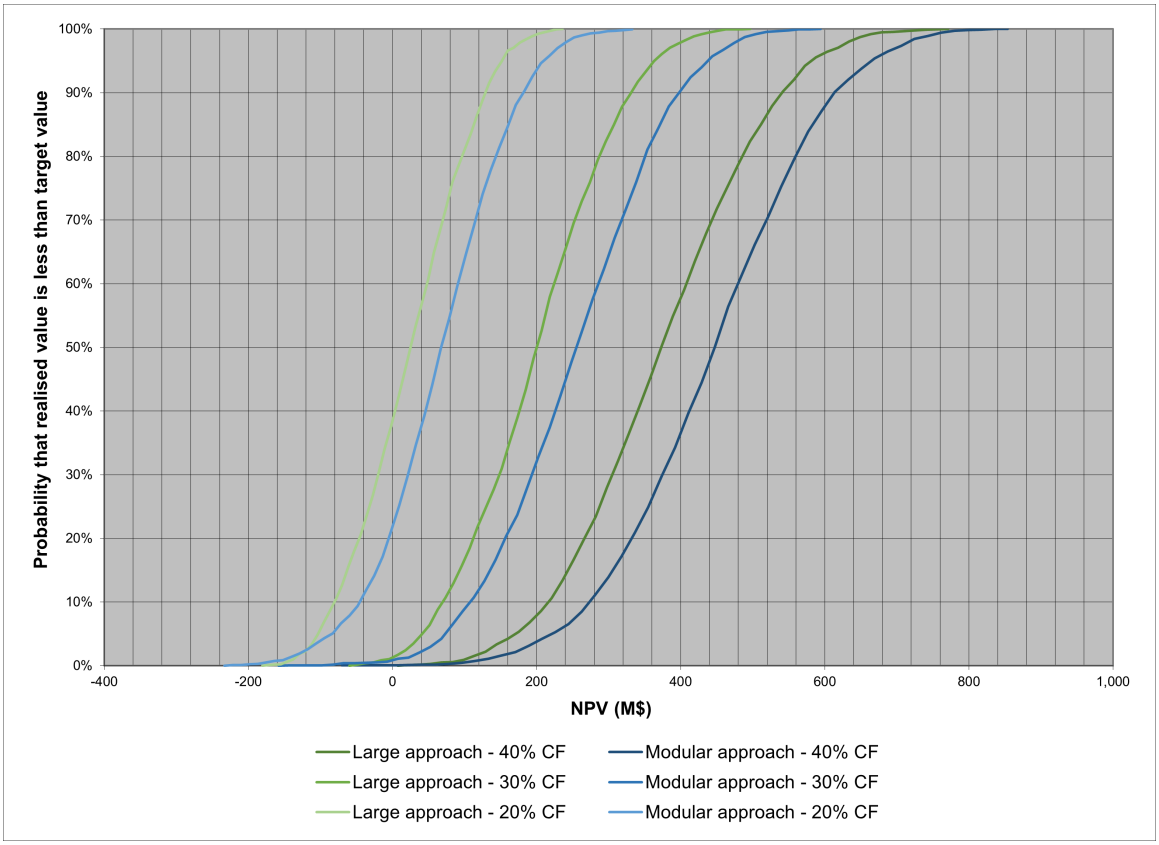

Figure 4-14: Target curve for NPV for Daggett, CA. The "build modular" approach CF curves are in shades of blue, while the "build large" approach CF curves are in shades of green.

Capacity Factor	0.2		0.3		0.4	
Dimension ($M)	Large approach	Modular approach	Large approach	Modular approach	Large approach	Modular approach
ENPV (P50 NPV)	27	67	199	251	373	447
Standard deviation	78	90	101	110	127	136
Value at risk (P5 NPV)	-99	-84	30	64	160	216
Value at gain (P95 NPV)	154	210	368	422	577	664
Initial capital expenditure	334	171	370	183	406	197

Figure 4-15: Multidimensional evaluation of the "build large" and "build modular" approaches for different CFs in Daggett, CA. Preferred values are shown highlighted.

4.5.5 Results for New Orleans, LA

The output of the stochastic simulation is a target curve showing a cumulative distribution of NPVs and their probability in the following figure 4-16. In the figure, the "build modular" approaches clearly dominate the "build large" approach at every CF. As the CF increases, the curves don't always shift to the right. This is probably because higher CFs require an exponential increase in heliostat area due to the poor solar resource, so the cost of the plant increases faster than the additional revenue generated by operating at a higher CF. Regardless, the "build modular" approach target curve beats the "build large" approach target curve in every selected dimension. These dimensions are shown in the following figure 4-17. In this figure 4-17, the "build modular" approach is favorable compared to the "build large" approach in all dimensions. However, it should be noted that all of the values are very negative.

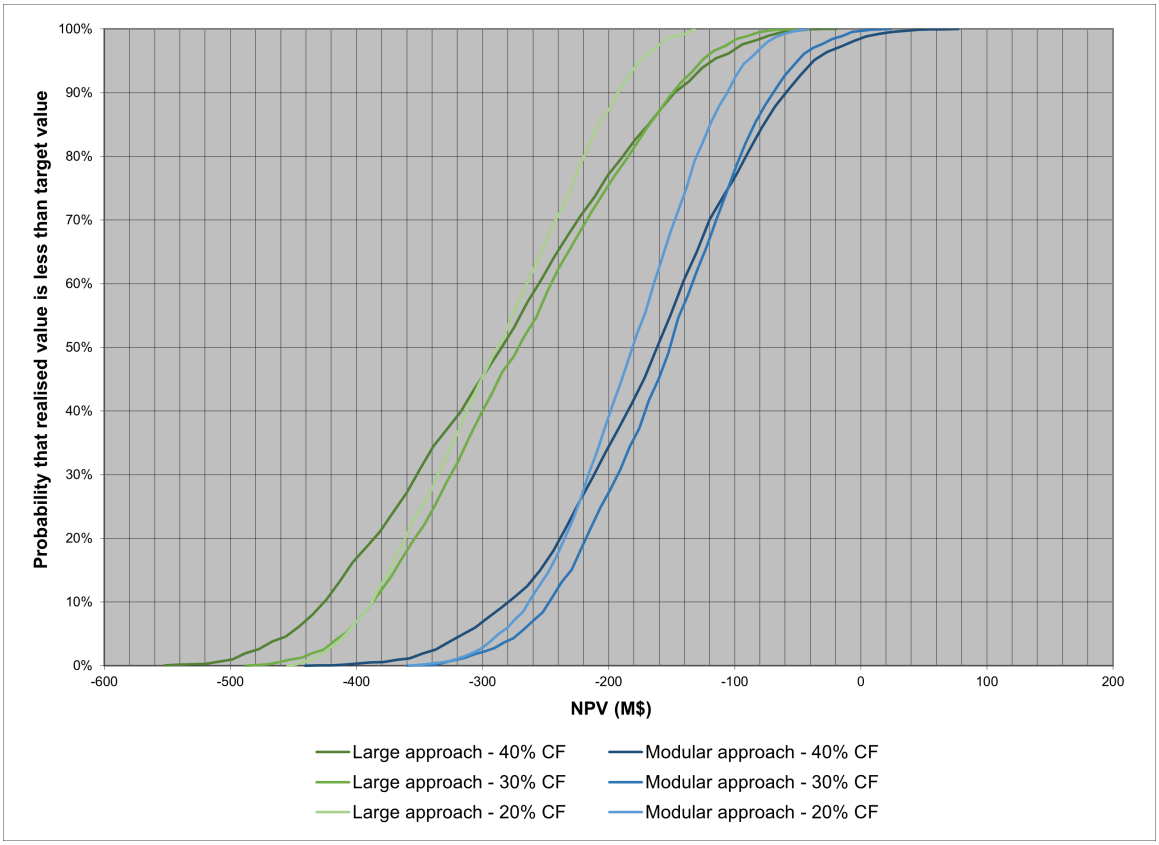

Figure 4-16: Target curve for NPV for New Orleans, LA. The "build modular" approach CF curves are in shades of blue, while the "build large" approach CF curves are in shades of green.

Capacity Factor	0.2		0.3		0.4	
Dimension ($M)	Large approach	Modular approach	Large approach	Modular approach	Large approach	Modular approach
ENPV (P50 NPV)	-289	-183	-270	-160	-286	-164
Standard deviation	74	60	86	68	106	83
Value at risk (P5 NPV)	-410	-286	-409	-276	-455	-308
Value at gain (P95 NPV)	-171	-90	-130	-56	-109	-32
Initial capital expenditure	382	59.3	436	65.5	519	78.2

Figure 4-17: Multidimensional evaluation of the "build large" and "build modular" approaches for different CFs in New Orleans, LA. Preferred values are shown highlighted.

4.5.6 Results for Boston, MA

The outputs for Boston, MA share multiple similarities with the results for Daggett, CA. The output of the stochastic simulation is a target curve showing a cumulative distribution of NPVs and their probability in the following figure 4-18. In the figure, the "build modular" approaches clearly dominate the "build large" approach at every CF. As the CF increases, the curves shift to the right, but the "build modular" approach target curve beats the "build large" approach target curve in nearly all of the selected dimensions. These dimensions are shown in the following figure 4-19. In this figure 4-19, the "build modular" approach is favorable compared to the "build large" approach in all dimensions except for the standard deviation, indicating the "build large" approach is relatively more robust than the "build modular" approach.

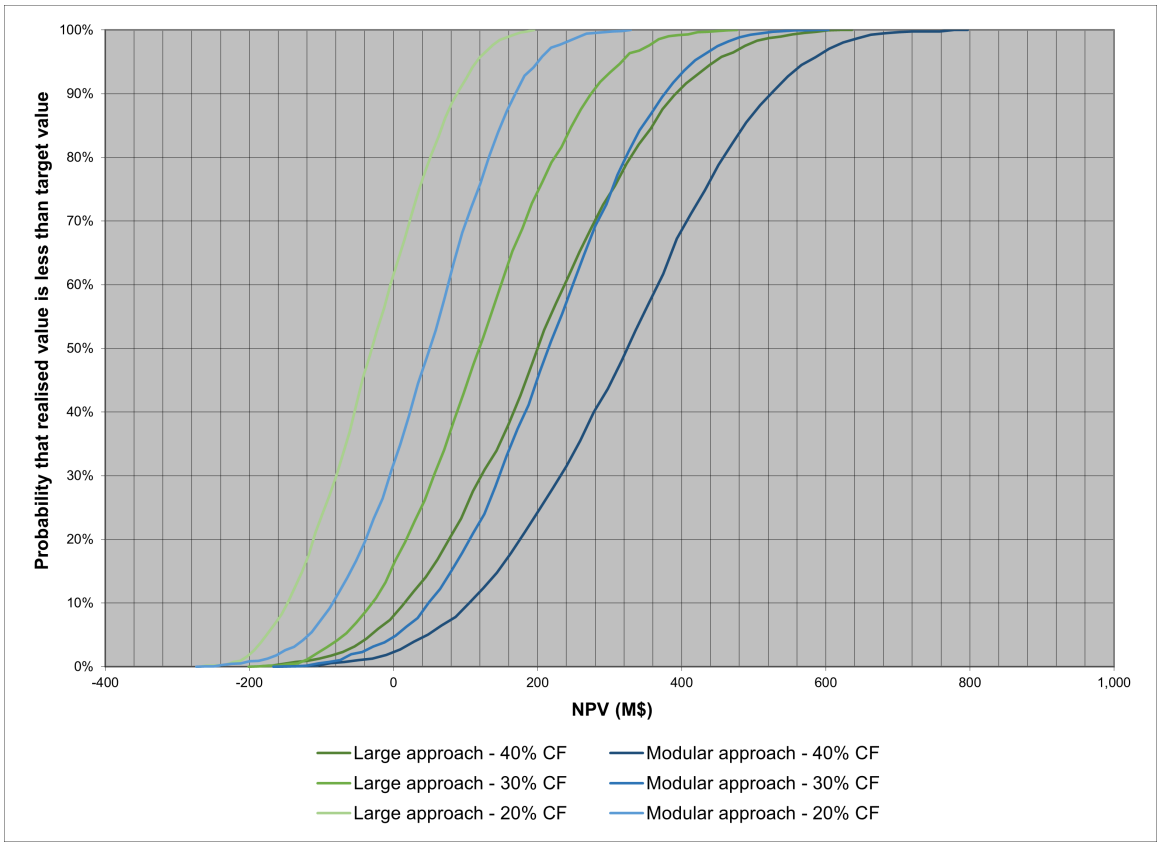

Figure 4-18: Target curve for NPV for Boston, MA. The "build modular" approach CF curves are in shades of blue, while the "build large" approach CF curves are in shades of green.

Capacity Factor	0.2		0.3		0.4	
Dimension ($M)	Large approach	Modular approach	Large approach	Modular approach	Large approach	Modular approach
ENPV (P50 NPV)	-26	49	119	210	202	315
Standard deviation	87	97	115	122	150	159
Value at risk (P5 NPV)	-166	-122	-68	5.7	-42	50
Value at gain (P95 NPV)	118	200	313	410	450	572
Initial capital expenditure	396	192	461	215	577	273

Figure 4-19: Multidimensional evaluation of the "build large" and "build modular" approaches for different CFs in Boston, MA. Preferred values are shown highlighted.

Chapter 5

Conclusion

5.1 Revisiting the key research questions

The central focus of this work was to compare the more rigid, conventional "build large" approach and the yet unproven, more flexible "build modular" approach for the deployment of hypothetical Gen3 solar tower CSP plants, using NPV as the metric by which the two approaches are compared.

Detailed performance and cost models were developed to provide inputs into the NPV analysis. The performance model was done in Modelon Impact and allowed the state of a Gen3 solar tower CSP plant to be tracked over an entire TMY. This model not only simulated the performance of the hardware comprisng the plant but also the performance of the software controlling the plant and ensuring the plant stayed within reasonable operating constraints during the entire TMY. These models were validated against real Gen1 and Gen2 solar tower CSP plants to ensure the heliostat field area required for each case was reasonable. The cost model was done in Microsoft Excel and used correlations available in public literature to estimate the costs of the components in the Gen3 solar tower CSP plants. Although detailed cost data for existing CSP plants is not available to compare directly and Gen3 solar tower CSP plants don't exist commercially yet, the cost model was used to generate estimated LCOEs of the hypothetical Gen3 solar tower CSP plants simulated in Modelon Impact. These estimated LCOEs were in line with current CSP industry data.

Under deterministic conditions, the "build large" approach appeared to be more favored as it generally yielded a higher NPV than the "build modular" approach. This aligns with most conventional industry knowledge about CSP, solar power plants, and power plants in general. Although the discount rate and the learning rate directionally support the "build modular" approach, the effects of these two do not outweigh the economies of scale for the "build large" approach (see figure 5-1 below). This is especially the case when the learning rate (0.1) is conservatively assumed to be fixed at the lower end of what is reported in literature about CSP. In the cost correlations, the economy of scale exponent α ranges between 0.4 and 0.8 for the sCO_2 power block equipment, so "larger" equipment (in the 100 MW_e power block, for example) is much more cost-effective than equipment in the smaller 10 MW_e power block. Lastly, because the profile of demand growth is already known in advance in the deterministic case, there is no value in the flexibility of building additional modules only when they are needed to meet demand. However, the real world seldom behaves

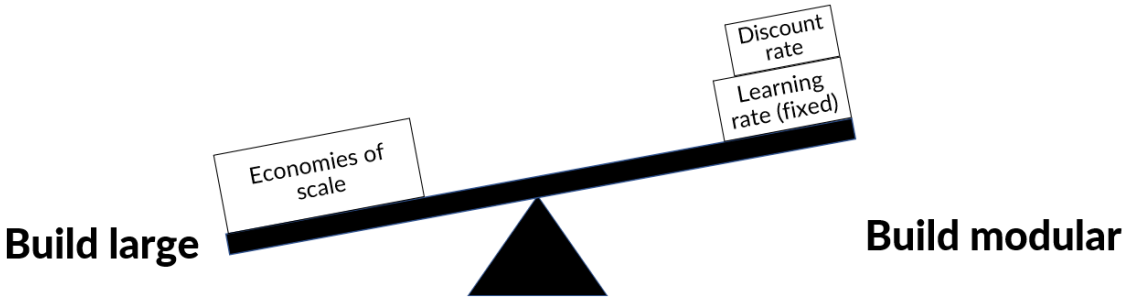

Figure 5-1: In deterministic conditions, the "build large" approach is favored.

in a deterministic manner where the future behavior of every variable that affects the performance of a system is known. There is uncertainty in the estimates of how variables behave in the future. Rather than using deterministic estimates, it is more useful to describe the future behavior of these variables using a random probability distribution. In a Gen3 solar tower CSP plant, there is uncertainty in not only environmental variables (such as how quickly the demand for electricity grows, the price of electricity, and variability in the solar resource) but also system variables such as the learning rate for modules and the cost of the plant. For some of variables, such as the price of variability, it is equally as likely that they are lower than expected as

they are higher than expected. However, for other variables, such as the cost of the plant, it is more likely that that the cost is higher than expected as opposed to lower than expected.

The case of the learning rate deserves special mention. In this work, the learning rate is one of the variables that is assumed to be more likely to be higher than expected than lower. Although multiple sources in literature quote values in the range of a conservative 10% for the learning rate of CSP, several of these studies are several years old at this point. The learning rate is well known and validated for a similar solar technology, solar PV, so it is natural to assume that the learning rate of CSP is known as well. However, there are a few key differences between solar PV and CSP. First, solar PV appears to be in a "takeoff" stage in terms of the rate of installed solar PV capacity around the world, but CSP seems to be lagging significantly behind. Second, the form of solar PV (panels) has been stable for more than one hundred years, while CSP is comparatively much more unstable - it has several variants and subvariants, and it is not clear which of these is dominant yet. In light of these differences, it is possible that a more rapid learning rate is possible, and data on the rate at which specific capital costs of all types of CSP plants have declined in the past few years supports this. This work has chosen the Gen3 solar tower CSP variant, which has been developed within the last few years. The Gen3 solar tower CSP plant concept has several advantages over competing subvariants and variants, including a higher theoretical maximum system efficiency and an architecture that centralizes the components that benefit most from centralizing (the power generation block and heat transfer fluid movement pathway) and decentralizes the components that benefit most from decentralizing (the heliostat field).

After incorporating uncertainty into the NPV simulation, the "build modular" approach is the preferred approach as it yields a higher ENPV, P5 NPV and P95 NPV than the "build large" approach while also requiring less initial capital investment. Although the "build large" approach is slightly more robust, the "build modular" approach is still recommended as it delivers between 10% and 30% more ENPV than the "build large" approach at 40%-50% less initial capital. The reduction in initial

capital alone could be highly valuable to firms that want to enter the market for baseload renewable energy via CSP, so the lowest number of starting modules that still generated a reasonably high ENPV (but not necessarily the maximum ENPV possible) was selected for most of the cases. Although the economies of scale still benefit the "build large" approach, the uncertainty in the cost of the plant diminishes this potential advantage over the "build modular" approach. For the "build modular" approach, the learning rate is allowed to be anywhere from 0.1 to 0.3, which greatly reduces the cost of multiple modules. Furthermore, the flexible build strategy for the modules allows modules to be built only when the demand calls for them and not sooner. It is clear that the "build modular" approach has benefited from the introduction of uncertainty while the "build large" approach has comparatively suffered from it. As a result, the effect of the variable learning rate, flexibility, and the discount rate inherent to the "build modular" approach outweigh the economies of scale for the "build large" approach (see figure 5-2). The pattern of the "build modular" approach

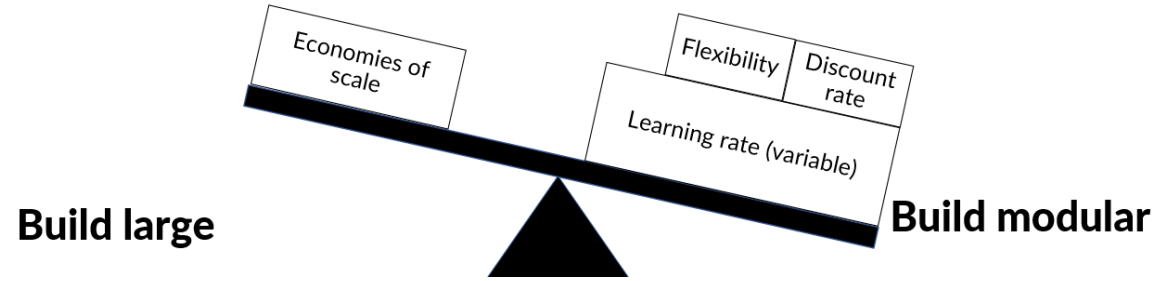

Figure 5-2: When uncertainty is introduced, the "build modular" approach is favored.

outperforming the "build large" approach in most categories of interest was observed in all three locations of interest in this work: Daggett, Boston, and New Orleans. It was no surprise that CSP plants had a high NPV in Daggett, CA, given the region's high solar resource and higher residential electricity prices. Between New Orleans and Boston, which have a similar (relatively poor) solar resource, the outcomes were very different. CSP was not at all favored in New Orleans even with a "build modular" approach, mainly due to the high cost of the plant (derived from the poor solar resource) and the low price of residential electricity. Interestingly, Boston, which has a poor solar resource, showed positive and potentially attractive NPVs despite the

poor solar resource and high cost of the plant. These negative effects were outweighed by the higher price of residential electricity in the region, making CSP a potentially viable option for Boston, especially if the modular approach is adopted.

In summary, for a firm that is looking to enter the CSP industry, a "build modular" approach is recommended over a "build large" approach, but only under certain conditions. First, the firm must make an effort to realize a high learning rate for its CSP technology, including learning by doing and learning by repetition. This requires an intentional focus on commonality between modules and their components over time. Without this focus, a CSP technology development and deployment approach that focused on bespoke or one-off designs in a "build modular" approach would not only lose on economies of scale relative to a "build large" approach but also would likely not be able to make a high learning rate a reality. Second, the firm must also make an effort to realize high flexibility for its CSP technology. The assumption in this work is that modules can be built and generating power in one year. However, if modules take longer to build and generate power, then the yearly demand for electricity cannot be matched so closely leading to either overcapacity for low demand or undercapacity for high demand - both of which negatively impact the NPV. This is not only a problem internal to the firm but also external to the firm as well. If a modular approach is employed, external stakeholders such as local communities, different levels and branches of government, etc. need to be supportive of the effort to gradually consume more land over time. In a worst case scenario, a firm could adopt a modular approach but then be blocked from expanding after year 1 by external stakeholders.

5.2 Future work

Future work could include the following:

- Performance model - improvements in the performance model would better estimate the performance of a Gen3 solar tower CSP plant, of which there are no commercial implementations yet. For example:

  - More accurate component models - for example, receiver efficiency as a function of variable external temperature, wind speed, and others. Inclusion and more rigorous models of heat losses through equipment like the silos and the particle lift, etc.
  - Heliostat field design - inclusion of more rigorous models of the heliostat field design and optimization

- Cost model - additional corroboration to Gen3 solar tower CSP plant component cost models, for which few exist in literature today. One particular opportunity area is the cost of the PHX and the equipment in the sCO_2 power block, both of which have a significant effect on the total plant.

- NPV model
  - Special focus should be on reducing the uncertainty around the learning rate for CSP, especially Gen3 solar tower CSP. Although there isn't any or enough commercial data on this variant, a mechanistic model could be developed to simulate the learning rate of this technology based on its components and the connectivity between these components.
  - This model was targeted towards the production of residential electricity. However, other business models could exist, and this approach could be adapted to simulate these, both deterministically and with uncertainty.

Bibliography

[1] IRENA (2021). Renewable Power Generation Costs in 2020. Technical report, The International Renewable Energy Agency, Abu Dhabi, 2021.

[2] IRENA (2022). Renewable Energy Statistics 2022. Technical report, The International Renewable Energy Agency, Abu Dhabi, 2022.

[3] Kevin J. Albrecht and Clifford K. Ho. Design and operating considerations for a shell-and-plate, moving packedbed, particle-to-sCO2 heat exchanger. *Solar Energy*, 178:331–340, November 2018.

[4] Mark Boslet. Is Ivanpah the World's Most Efficient Solar Plant?, June 2010. Section: Solar.

[5] Christian Breyer, Svetlana Afanasyeva, and Dietmar Brakemeier. Assessment of mid-term growth assumptions and learning rates for comparative studies of CSP and hybrid PV-battery power plant. In *AIP Conference Proceedings 1850*. AIR Publishing, 2017.

[6] Reiner Buck and Stefano Giuliano. Impact of Solar Tower Design Parameters on sCO2-based Solar Tower Plants. Essen, Germany, 2018. DuEPublico.

[7] Ka Man Chung, Jian Zeng, Sarath Reddy Adapa, Tianshi Feng, Malavika V. Bagepalli, Peter G. Loutzenhiser, Kevin J. Albrecht, Clifford K. Ho, and Renkun Chen. Measurement and analysis of thermal conductivity of ceramic particle beds for solar thermal energy storage. *Solar Energy Materials and Solar Cells*, 230, September 2021.

[8] Aalborg CSP. History of CSP.

[9] Richard de Neufville and Stefan Scholtes. *Flexibility in Engineering Design*. The MIT Press, August 2011.

[10] Olivier L. de Weck. *Technology Roadmapping and Development: A Quantitative Approach to the Management of Technology (pre-publication draft)*. Springer Nature, 2021.

[11] John A. Duffie and William A. Beckman. *Solar Engineering of Thermal Processes*. Wiley, fourth edition edition, 2013.

[12] John Dyreby, Sanford Klein, Gregory Nellis, and Douglas Reindl. Design Considerations for Supercritical Carbon Dioxide Brayton Cycles With Recompression. *Journal of Engineering for Gas Turbines and Power*, 136, October 2014.

[13] John J. Dyreby. *Modeling the Supercritical Carbon Dioxide Brayton Cycle with Recompression*. PhD thesis, University of Wisconsin-Madison, 2014.

[14] B. Ehrhart and D. Gill. Evaluation of Annual Efficiencies of High Temperature Central Receiver Concentrated Solar Power Plants with Thermal Energy Storage. *Energy Procedia*, 49(2014):752–761, 2014.

[15] US EIA. Electricity use in homes - U.S. Energy Information Administration (EIA), May 2019.

[16] Energy.gov. SCO2 Power Cycles.

[17] Institute for Advanced Sustainability Studies. CN | Concentrating Solar Power Projects | NREL, 2021.

[18] Institute for Advanced Sustainability Studies. Crescent Dunes Solar Energy Project | Concentrating Solar Power Projects | NREL, 2021.

[19] Abel Gustafson, Matthew Goldberg, Seth Rosenthal, John Kotcher, Edward Maibach, and Anthony Leiserowitz. Who is willing to pay more for renewable energy?, July 2019.

[20] Lukas Heller, Stefan Glos, and Reiner Buck. SCO2 POWER CYCLE DESIGN WITHOUT HEAT SOURCE LIMITATIONS: SOLAR THERMAL PARTICLE TECHNOLOGY IN THE CARBOSOLA PROJECT. Online, 2021. DuEPublico.

[21] Lukas Heller, Stefan Glos, and Reiner Buck. Techno-economic selection and initial evaluation of supercritical CO2 cycles for particle technology-based concentrating solar power plants. *Renewable Energy*, 181(2022):833–842, September 2021.

[22] Md Tasbirul Islam, Nazmul Huda, A.B. Abdullah, and R. Saidur. A comprehensive review of state-of-the-art concentrating solar power (CSP) technologies: Current status and research trends. *Renewable and Sustainable Energy Reviews*, 91:987–1018, 2018.

[23] J.E. Haysom, O. Jafarieh, H. Anis, K. Hinzer, and D. Wright. Learning curve analysis of concentrated photovoltaic systems. *Prog. Photovolt: Res. Appl.*, 23:1678–1686, 2015.

[24] Christoph Kost, Johannes N. Mayer, and Jessica Thomsen. Levelized Cost of Electricity - Renewable Energy Technologies. Technical report, Fraunhofer Institut for Solar Energy Systems ISE, November 2013.

[25] Lazard. Lazard's Levelized Cost of Storage Analysis - Version 4.0. Technical report, Lazard, 2018.

[26] Johan Lilliestam, Merce Labordena, Anthony Patt, and Stefan Pfenninger. Empirically observed learning rates for concentrating solar power and their responses to regime change. *Nature Energy*, 2(17094), 2017.

[27] Smithsonian Magazine. A Brief History of Solar Panels. Section: Sponsored, Innovation, , Energy, , Articles.

[28] Conor McGlade. Exploring the Crescent Dunes Solar Energy Plant, October 2018.

[29] Mark Mehos, Craig Turchi, Judith Vidal, Michael Wagner, Zhiwen Ma, Clifford Ho, William Kolb, Charles Andraka, and Alan Kruizenga. Concentrating Solar Power Gen3 Demonstration Roadmap. Technical Report NREL/TP-5500-67464, National Renewable Energy Laboratory, January 2017.

[30] L. Neij. Cost development of future technologies for power generation – A study based on experience curves and complementary bottom-up assessments. *Energy Policy*, 36:2200–2211, 2008.

[31] Kenneth E. Nichols. How to Select Turbomachinery For Your Application. Technical report, Barber Nichols, November 2019.

[32] NREL. NSRDB Data Viewer.

[33] NREL. System Advisor Model (SAM), 2021.

[34] Gary E. Rochau. Supercritical CO2 Brayton Cycle Development, June 2014.

[35] Jose Santamarta. How Concentrated Solar Power Works: Tower, Trough, Fresnel or Dish.

[36] Sargent and Lundy. Assessment of Parabolic Trough, Power Tower and Dish Solar Technology Cost and Performance Forecasts – 2008. Technical report, US Department of Energy and Sandia Laboratory, 2009.

[37] US Department of Energy Solar Energy Technologies Office. Generation 3 Concentrating Solar Power Systems (Gen3 CSP) Phase 3 Project Selection.

[38] Roland Span and Wolfgang Wagner. A New Equation of State for Carbon Dioxide Covering the Fluid Region from the Triple-Point Temperature to 1100 K at Pressures up to 800 MPa. Journal of Physical and Chemical Reference Data 25(1509), 1996.

[39] Georgia Tech. Carbo HSP 40/70 – Thermophysical Properties Database of Gen3 CSP Materials.

[40] Jessika E. Trancik. Technology improvement and emissions reductions as mutually reinforcing efforts: Observations from the global development of solar and wind energy. Technical report, Massachusetts Institute of Technology, November 2015.

[41] Irene Tzinis. Technology Readiness Level, May 2015. Publisher: Brian Dunbar.

[42] Lund University. [NEEDS] – New Energy Externalities Developments for Sustainability, Cost development – an analysis based on experience curves. Technical Report D 3.3 - RS 1a, Lund University, 2006.

[43] U.S. Bureau of Labor Statistics. Average Price: Electricity per Kilowatt-Hour in Boston-Cambridge-Newton, MA-NH (CBSA), November 1978. Publisher: FRED, Federal Reserve Bank of St. Louis.

[44] U.S. Bureau of Labor Statistics. Average Price: Electricity per Kilowatt-Hour in Riverside-San Bernardino-Ontario, CA (CBSA), January 2018. Publisher: FRED, Federal Reserve Bank of St. Louis.

[45] Nathan T. Weiland, Blake Lance, and Sandeep R. Pidaparti. SCO2 POWER CYCLE COMPONENT COST CORRELATIONS FROM DOE DATA SPANNING MULTIPLE SCALES AND APPLICATIONS. In *ASME Turbo Expo 2019*, Phoenix, Arizona, 2019. ASME.

[46] Wikipedia. Crescent Dunes Solar Energy Project, April 2022. Page Version ID: 1085286695.

[47] Wikipedia. Ivanpah Solar Power Facility, April 2022. Page Version ID: 1083323821.

[48] Stephen Wilcox and Christian A. Gueymard. SPATIAL AND TEMPORAL VARIABILITY OF THE SOLAR RESOURCE IN THE UNITED STATES. Technical report, National Renewable Energy Laboratory.

[49] T.P. Wright. Factors Affecting the Cost of Airplanes. In *Journal of the Aeronautical Sciences*, 1936.

[50] Alex Zdanov. Entergy New Orleans: Rates, Coverage Area, Emissions.

[51] Qian Zhu. Power generation from coal using supercritical CO2 cycle. Technical Report CCC\280, IEA Clean Coal Centre, December 2017.